PAVING THE SEAFLOOR: VOLCANIC EMPLACEMENT PROCESSES DURING THE 2005–06 ERUPTION AT THE FAST-SPREADING EAST PACFIC RISE, 9˚50′N

By

ALLISON TREMBLAY FUNDIS

A THESIS PRESENTED TO THE GRADUATE SCHOOL
OF THE UNIVERSITY OF FLORIDA IN PARTIAL FULFILLMENT
OF THE REQUIREMENTS FOR THE DEGREE OF
MASTER OF SCIENCE

UNIVERSITY OF FLORIDA

2010

To Stein

ACKNOWLEDGMENTS

I am in great debt to a number of friends and colleagues who provided analytical, financial and mental support during the realization of my masters research. My greatest thanks go to Mike Perfit, for his guidance and financial support throughout the completion of this thesis. I would also like to thank Pete Adams and Ray Russo for their support as committee members. A great deal of thanks goes to Adam Soule and Daniel Fornari, for their constant inspiration, guidance and assistance with data interpretation. I want to especially thank Dan for taking me out on my first research cruise three years ago and inspiring me to fall in love with geology.

Many thanks are due to the scientists and crew involved in collecting data during the NH06, AT15-6, AT15-13, AT15-15 and AT15-27 cruises on the R/V New Horizon and the R/V Atlantis, especially Dan Fornari, Adam Soule, Karen Von Damm and Marshall Swartz.

This research would not have been completed without the financial support of a NSF grant and the mental support provided by my family and friends.

TABLE OF CONTENTS

page

ACKNOWLEDGMENTS 4

LIST OF FIGURES 6

ABSTRACT 7

CHAPTER

1 INTRODUCTION 8

2 BACKGROUND 11

3 METHODS 14

Deep-towed Camera Surveys 14
Image Analysis 15
Sidescan Sonar Mapping 16
Analytical Methods 16

4 RESULTS 22

Abundance of Lava Morphologies 22
Morphological Transitions 22
Distribution of Volcanic Structures 25
Collapse Pits 25
Kipukas 26
Faults and Fissures 27
Sidescan Sonar Imagery 27

5 DISCUSSION 36

Influence of Pre-existing Slope and Terrain on Surface Morphology 36
Pre-existing Slope Analysis 38
Pre-existing Morphology Analysis 38
Evidence of High Eruption Rates for the 2005–06 Eruption 39
Eruption Length and Distribution of Morphology Along Axis 40
Distribution of Morphology Across Axis 41

6 CONCLUSIONS 45

APPENDIX TOWCAM PROFILES 46

LIST OF REFERENCES 50

BIOGRAPHICAL SKETCH 56

LIST OF FIGURES

Figure page

1-1. Location and bathymetry of the East Pacific Rise 9˚50´N 10

3-1. Area of the 2005–06 eruption surveyed with TowCam 18

3-2. Examples of classification scheme used for the survey images. 19

3-3. Distribution of the four main types of morphology of the 2005–06 eruption 20

3-4. Distribution of collapse and kipukas within the 2005–06 eruption....21

4-1. Observations of morphology and collapse binned by latitude 29

4-2. Pillow flows and kipukas relative to proximity to the 2005–06 flow boundary 30

4-3. Examples of transitions between different morphologies of the 2005–06 flow....31

4-4. Collapse relative to proximity to the AST....32

4-5. Evidence that subsurface pathways were utilized by the 2005–06 flows....33

4-6. Evidence of lava-vapor interaction in handsample....34

4-7. Sidescan sonar imagery collected in 2007 overlain with observations from TowCam surveys 35

5-1. Lava morphology plotted as a function of pre-existing slope 43

5-2. Comparison of pre-eruption and post-eruption morphology....44

A-1. TowCam survey AT15-6:CT02 bottom profile and post-eruption slope 46

A-2. TowCam survey AT15-6:CT06 bottom profile and post-eruption slope 47

A-3. TowCam survey AT15-13:CT01 bottom profile and post-eruption slope 48

A-4. TowCam survey AT15-13:CT02 bottom profile and post-eruption slope 49

Abstract of Thesis Presented to the Graduate School
of the University of Florida in Partial Fulfillment of the
Requirements for the Degree of Master of Science

PAVING THE SEAFLOOR: VOLCANIC EMPLACEMENT PROCESSES DURING THE 2005–06 ERUPTION AT THE FAST-SPREADING EAST PACIFIC RISE, 9°50′N

By

Allison Tremblay Fundis

May 2010

Chair: Michael Perfit
Major: Geology

The 2005–06 eruption near 9°50′N marked the first observed repeat eruption at a mid-ocean ridge and provided a unique opportunity to deduce the emplacement dynamics of a single eruptive event. Since this new flow was documented in April 2006, a total of 40 deep-towed imaging surveys have been conducted with the Woods Hole Oceanographic Institution's (WHOI) TowCam system. These surveys collected more than 60,000 digital color images and high-resolution (1 m vertical resolution) bathymetric profiles. Our analyses quantify the spatial distributions of lava flow surface morphologies and allow us to investigate how these various morphologies relate to the physical characteristics of the ridge and dynamics of flow emplacement. Images of the 2005–06 flows from each of the TowCam surveys were analyzed for lava flow morphology and for the presence of kipukas, collapse, faults and fissures. Our analysis of the distribution of lava morphology emplaced during this eruption shows that lava effusion rate was the dominant factor controlling the observed morphological variations in the 2005–06 flows. We also show that effusion rates were higher than in previously studied eruptions at this site and were variable along the length of the eruptive fissure. The 2005–06 eruption at the fast-spreading EPR is characterized by 52% lobate flows, 31% sheet flows, 14% hackly flows and 2% pillow flows.

CHAPTER 1
INTRODUCTION

Submarine volcanic eruptions at mid-ocean ridges (MOR) are responsible for creating >70% of the planet's crust, yet, our understanding of volcanic processes in these settings has been limited by our inability to directly observe active eruptions. During the course of the past few decades of high-resolution seafloor mapping, only a few seafloor volcanic eruptions have been well documented [*Embley et al.,* 1990, 1995; *Chadwick et al.,* 1991, 1995; *Haymon et al.,* 1993*; Rubin et al*., 1994; *Gregg et al.,* 1996; *Sinton et al.,* 2002], and in most cases there are gaps in our knowledge of both the size and continuity of individual lava flows that comprise the eruptive episodes. Volcanic deposition and tectonic disruption at MOR axes greatly impact the permeability and structure of the upper oceanic crust, and thus the hydrothermal systems driven by fluid flow within the shallow crust. It is therefore important to understand the mechanisms responsible for lava emplacement and deposition at MOR settings. This study examines in detail the erupted products of a single submarine eruption in order to place constraints on the mechanisms responsible for emplacement and deposition of lava on the seafloor at a fast-spreading MOR through lava flow surface morphology and intraflow features.

In 2006, an eruption centered near the magmatically robust 9°50′N region of the East Pacific Rise (EPR) was discovered and the flow area fully mapped [*Soule et al*., 2007a] (Figure 1-1). Microseismicity data, Po-disequilibrium dating, and continuous time-series temperature records collected at nearby hydrothermal vents indicate that the eruption occurred as a series of pulses between mid-2005 to January 2006 [*Tolstoy et al.,* 2006; *Cowen et al.,* 2007; *Soule et al.,* 2007a; *Rubin et al.,* 2006, 2008, in prep; *Von Damm et al*., in prep.]. This discovery and subsequent investigations of the geological, hydrothermal and biological impacts of the eruptions provide the first documented evidence for a repeat eruption at a MOR site, in agreement with

predictions of decadal recurrence intervals at this fast-spreading ridge [*Haymon et al*., 1993; *Perfit and Chadwick*, 1998].

The parameters that control submarine lava surface morphology differ from those that control subaerial flows. In submarine environments, lava temperature and crystal content remain relatively constant due to the rapid formation of a thick and insulating crust [*Gregg et al.*, 1998; *Fornari et al.,* 2004] and thus, do not change the rheology of the lava and the subsequent manner in which the lava surface deforms [e.g., *Soule et al.,* 2004]. Studies using wax models have shown that surface morphology is dependent on the timescales of cooling and advection [*Fink and Griffiths*, 1992; *Gregg and Fink*, 2000; *Sakimoto and Gregg*, 2001]. Due to the significant thermal gradient between lava and seawater, cooling rates of submarine lavas with differing surface morphologies should be relatively similar. Thus, prior to this study, the dominant parameter believed to control surface morphology was the timescale of advection, which is a proxy for the local volume flux influenced by eruption rate and pre-existing topography [e.g., *Gregg and Fink*, 1998; *Sakimoto and Gregg*, 2001].

Here we use seafloor photography and high-resolution bathymetric profiles (1 m vertical precision) from deep-towed camera surveys and Alvin dive imagery, and sidescan imagery collected over the 2005–06 flows to produce a geologic map of the volcanic features associated with this most recent eruption at the EPR near 9°50′N. Our analysis of the distribution of lava morphology emplaced during this eruption shows that lava effusion rate was the dominant factor controlling the observed morphological variations in the 2005–06 flows at the EPR near 9°50′N. We also show that the effusion rates were higher than in previous studied eruptions at this site and were variable along the length of the eruptive fissure.

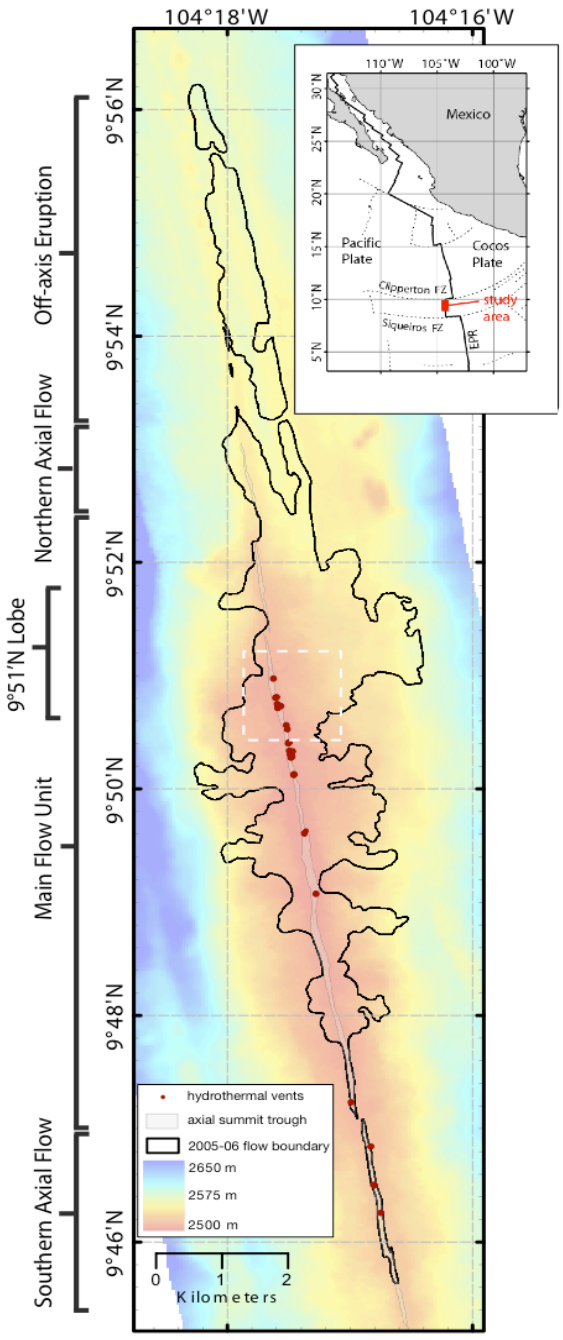

Figure 1-1. Location and bathymetry of the East Pacific Rise 9˚50´N. The 2005–06 eruption is outlined in black (derived from camera tow and sidescan imagery data) and the 4 distinct regions of the flow are defined. Hydrothermal vents are marked by red dots. The dashed white box refers to the location of Figure 4-7.

CHAPTER 2
BACKGROUND

The northern EPR between the Clipperton (~10°N) and Siqueiros (~8°30′N) transform faults is a fast-spreading [5.5 cm/yr [*Carbotte and Macdonald*, 1992)] MOR and one of the best studied segments of the global ridge system [e.g., *Lonsdale,* 1977; *Macdonald et al.*, 1984, 1992; *Langmuir et al.*, 1986; *Perfit et al.*, 1994; *Fornari et al.,* 1998, 2004; *Perfit and Chadwick*, 1998; *Soule et al.*, 2007a; *Escartin et al.*, 2007; *Goss et al.*, in review]. Over the past two decades, two documented eruptions have occurred along this segment of the EPR near the 9°50′N region, one in 1991-1992 [*Haymon et al.*, 1993; *Rubin et al*., 1994] and the most recent one in 2005–06 [*Tolstoy et al.*, 2006; *Rubin et al.*, 2006; *Cowen et al.,* 2007; *Soule et al.*, 2007a]. Using data from deep-sea camera surveys and Alvin dive traverses, *Soule et al*. [2007a] estimated that the 2005–06 eruption was 4-5 times more voluminous than the rough estimate for the 1991–92 eruption [*Gregg et al.*, 1996]. The 2005–06 eruptions were fed by eruptive fissures located within the axial summit trough (AST), which is the site of most of the primary eruptive fissures [*Fornari et al*., 1998, 2004] and known high- and low-temperature hydrothermal vents [e.g., *Haymon et al*., 1991; 1993; *Von Damm*, 1995; *Shank et al*., 1998], as well as a fissure system located ~ 700 m east of the EPR axis in the 9°53′–9°55′N region. As suggested by *Soule et al.*, [2007a], the mapped flow boundary indicates that multiple flow lobes were produced along the ~18 km eruptive fissure system between 9°46′N and 9°56′N, possibly reflecting discrete eruptive events [*Rubin et al.,* 2006, 2008] during the 2005–06 eruption. These lobes coincide with pre-existing, ~10–50 m wide east-west trending lava channels that have been interpreted by *Soule et al.* [2005] to have served as distribution pathways for axially erupted lavas. The largest of these lobes, between 9°50′N and 9°52′N, coincides with the highest density of high-temperature hydrothermal vents along the ridge [*Fornari et al.*, 2004; *Soule et al.*, 2007a], and for the

purpose of this study it is referred to as the 9°51′N lobe. The 2005–06 flows may be characterized by 4 distinct regions defined by their geology and mechanisms of flow emplacement: 1) the area referred to in this study as the 9°51′N lobe and main flow unit, 2) flow produced by smaller axial eruptions north of 9°53′N through a discontinuous series of fissures and axially sourced flow that was directed north by a ridge-parallel fault, 3) off axis flows erupted from fissures ~700 m east of the axis near 9°54.5′N, and 4) the area between 9°49′N and 9°46′N where a small volume of axially erupted flows, found largely in the AST have been identified [*Goss et al*., in review] (Figure 1-1).

In the past, our understanding of the size of eruptions and the relationship between flow morphologies and eruptive processes along the MOR system have been limited by our inability to distinguish individual eruptive units. The key difference between this study and studies of seafloor characterization of other MOR sites where eruptions have been documented [e.g., *Embley et al*., 1990; *Chadwick et al.*, 1991; *Sinton et al*., 2002] is that we were able to survey the area affected by the eruption comprehensively and shortly after the discovery. We surveyed the 2005–06 eruption with digital seafloor imaging on multiple cruises so that we could unequivocally establish the boundaries of the new flows and collect detailed bathymetric data and lava samples.

We use results from previous studies, including those presented in White et al., [2006] to help define the pre-existing lava morphology and topography in the study area, and to compare and contrast them to seafloor volcanic features created during the 2005–06 eruption. Prior to the 2005–06 eruption, *Kurras et al.* [2000] used imagery from Alvin and deep-towed camera surveys to interpret the volcanic history and lava emplacement processes at the EPR between 9°49′N and 9°52′N. They reported that the crest of the EPR was predominately covered by lobate (66%) and

sheet flows (20%), consistent with the idea that fast-spreading ridges typically produce high-effusion rate eruptions [*Perfit and Chadwick*, 1998]. Additionally, they reported that the 9°50′N area had experienced three types of volcanic emplacement processes including: (1) axial summit eruptions, (2) off-axis transport of axially erupted lava through channelized surface flows, and (3) off-axis eruptions. *Engels et al.* [2003] investigated the distribution and formation of collapse features observed on the EPR axis in the 9°37′N area and reported that collapse almost always occurred within lobate flows. Moreover, collapse pits <2 m in diameter were evenly distributed out to ~200 m from the AST, while collapse >2 m in diameter were concentrated within 100 m of the axis.

CHAPTER 3
METHODS

Deep-Towed Camera Surveys

A total of 40 deep-towed imaging surveys were conducted in the study area during 2006-2007 using the Woods Hole Oceanographic Institution's TowCam system [*Fornari*, 2003]. Approximately 60,000 digital color images were collected. Bathymetric profiles (1-m vertical precision) were compiled using a 100 kHz altimeter and depth acquired using the TowCam's SeaBird SBE25 CTD. The TowCam was equipped with a color digital camera (3.5 megapixel) for 30 of the tows and a fiber optic camera (4 megapixel) was used during two cruises (AT15-6 and AT15-27) for 10 tows. TowCam's speed over the bottom was typically $\leq$0.5 knots. Towing altitude was normally 5-7 meters above the seafloor, producing images that each cover an area of ~4.5 m x 6 m of seafloor when the color digital camera was in use and ~3.5 m x 3.5 m when the fiber optic system was utilized. Images were acquired at 10–15 seconds intervals, producing 0-20% of overlap between each successive image. During 18 surveys, the TowCam was navigated using a bottom-moored long baseline (LBL) transponder network [*Hunt et al.*, 1974; *Milne,* 1983; *Soule et al.*, 2007a] that located the images to within 5-8 meters [*Haymon et al.*, 1991; *Fornari et al.,* 1998]. During 22 of the surveys that were conducted outside the LBL network area, the TowCam was navigated using layback calculations that located the images to within ~100 meters [*Soule et al*., 2007a] (Figure 3-1). TowCam image data were supplemented by down-looking video imagery collected during post-eruption Alvin dives. Dives 4204 and 4296 traversed areas south of the off-axis flow near 9°53′N and dive 4205 traversed the southern extent of the eruption near 9°46′N.

Image Analysis

Each TowCam image was classified for relative age and lava flow morphology. Boundaries of the 2005–06 flows were easily identified by the lack of sediment on the flow surfaces and the presence of fresh glassy lava surfaces and provided the basis for coarse relative age estimates (2005–06 versus older). Lava flow surfaces in each of the images were classified into one of four morphological categories: pillow flow, lobate flow, sheet flow, and hackly flow, consistent with the descriptions used by *Ballard and Van Andel* [1977], *Ballard et al.* [1982] and *Kurras et al.* [2000] (Figure 3-2a-d). In instances where multiple morphologies were present in an image, the dominant morphology by area was recorded. Three morphologic types of sheet flow (lineated, ropy and hackly) were observed and all are indicative of high flow rates at the time of emplacement [*Gregg and Fink*, 1995*; Gregg et al.,* 1996; *Chadwick et al*., 1999]. Hackly flows were distinguished from other sheet flows because initial observations of the 2005–06 flow morphologies from the TowCam observations and Alvin dives indicated that this eruption produced a higher percentage of hackly flows than previously existed in the region, especially within the 9°51′N lobe. The discrimination of hackly flows from lineated and ropy sheet flows is used here to help refine the emplacement mechanisms involved in erupting the 2005–06 flows.

Images were also classified for the presence and abundance of collapse pits, kipukas (defined in this study as an area of exposed flow older than the 2005–06 flow and completely surrounded by the 2005–06 flow), faults, and fissures (Figure 3-2e-j). Collapse pits were classified into three size categories using the terminology and size classes described in *Engels et al.* [2003]: lobate blisters (<2 m diameter), skylights (~2–10 m diameter), and lava pond collapse (>10 m diameter). Kipukas were only recorded if they were identifiable in <3 image frames (ranging from <1 meter to ~6 meters in diameter). Potentially larger kipukas that are not easily

distinguished from true gaps in lava deposition were not included in our study. Faults and fissures were rare within the imaging surveys.

Sidescan Sonar Mapping

In April 2007, a near bottom sidescan sonar survey was conducted using a 120 kHz deep-towed sonar system towed at ~120 m altitude and a speed of 1.6 knots [*Soule et al.,* 2007b; *Scheirer et al*., 2000]. The survey comprised four track lines along a ~23 km segment of the EPR crest from 9°45′N to 9°58′N. Sidescan data were navigated using a layback calculation based on the sonar depth and wire out; the navigational precision is < 50 m, and the backscatter imagery was gridded at 2 m. The sidescan imagery was used in this study to examine how the various morphologies observed in the images correlate with the acoustic textures in the sidescan imagery.

Analytical Methods

Soule et al. [2007a] calculated the surface area of the 2005–06 flows to be ~14.6 km^2 based on the location of contacts between the 2005–06 flows and older flows determined from the initial TowCam survey images. Further interpretation of the sidescan imagery in conjunction with our analysis of the images has lead to a new estimate of ~16.7 km^2 for the surface area of the 2005–06 flows. We consider this to be a minimum of the flow surface area, however, because we have imaged the 2005–06 flow as far as ~3 km off-axis, which is ~1.2 km further away from the boundary of the 2007 sidescan sonar survey and the previously reported extent of the 2005–06 flow [*Soule et al*., 2007a].

Of ~60,000 images collected during recent TowCam surveys, about half (27,205 images) imaged the 2005–06 flows. Due to areas of extensive collapse in the new flow, it was not possible to classify the flow morphology in ~10% of these images (2,104 images). Assuming each TowCam image covered ~23 m^2 of seafloor on average, the camera surveys covered ~0.58

km^2 (25,101 images) of the 2005–06 flows. Images where morphologic and tectonic structures were classified represent less than 4% of the flow surface area. The surveys, however, evenly cover the extent of the 2005–06 flows along and across axis (Figure 2-2), and we thus consider our analyses to be representative of the entire 2005–06 flow.

Observations from the towed camera surveys were entered into a database and subsequently linked to time-stamped navigation and near-bottom profiles generated from the CTD depth and altitude data. These georeferenced observations were then compiled and used to plot distributions of the various lava flow morphologies and volcanic structures observed in the photographs (Figures 3-3 and 3-4).

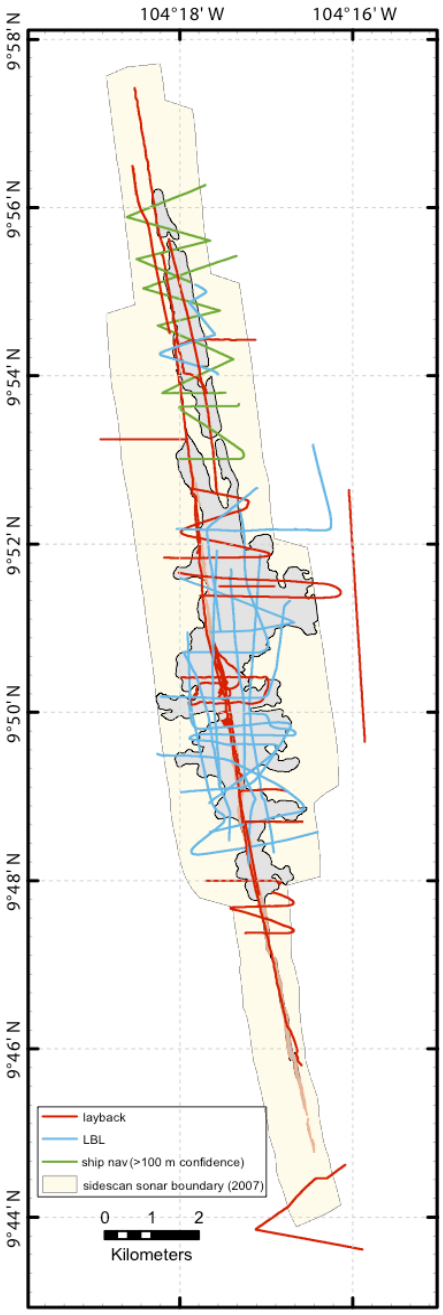

Figure 3-1. Tracklines showing area of the 2005–06 eruption surveyed with TowCam. Blue lines represent navigational precision of ~5 m, red lines represent ~100 m precision and the green lines represent >100 m precision. The yellow region shows the area covered by the DSL120-A sidescan sonar survey.

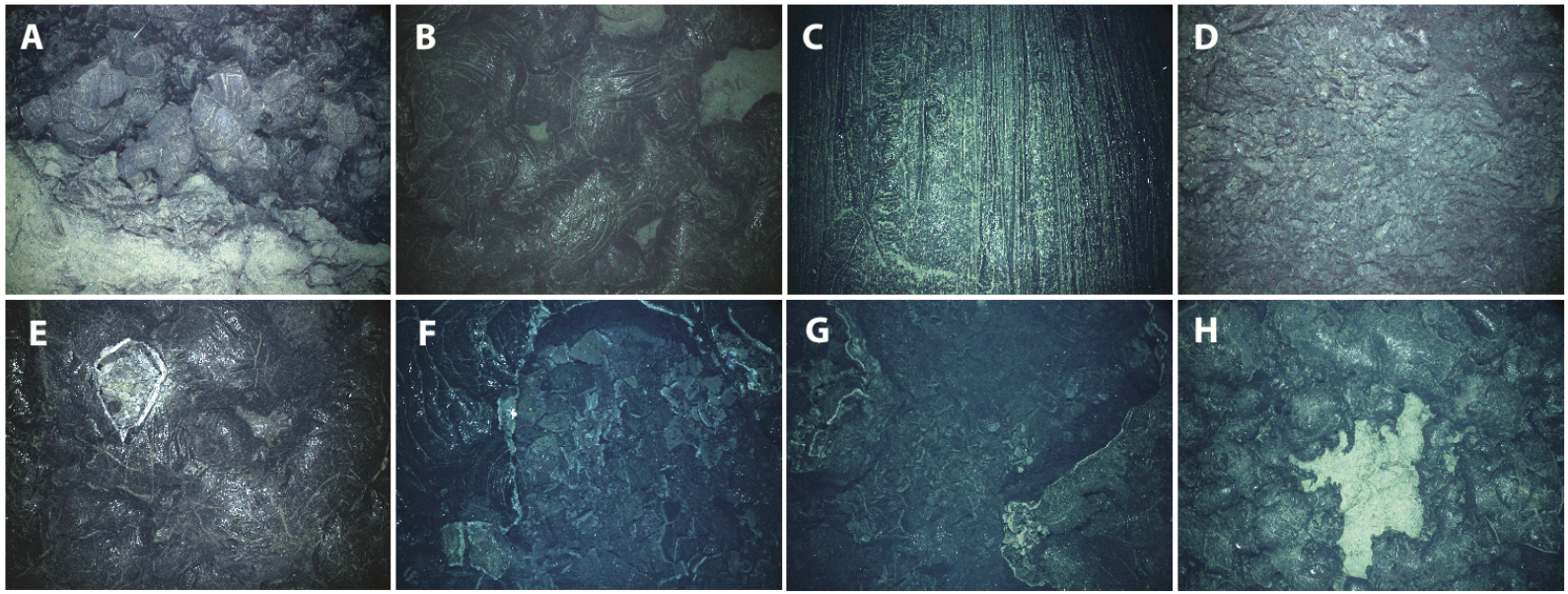

Figure 3-2. Images showing examples of classification scheme used for the survey images. A-D show the four morphology types: A) pillow, B) lobate, C) sheet and D) hackly. E-G show the three collapse types: E) lobate blisters, F) skylight collapse and G) lava pond collapse. H) Shows an example of a kipuka, an area of exposed flow older than the 2005–06 flow and completely surrounded by the 2005–06 flow. Horizontal scale across the bottom of each photograph is ~3–5 m.

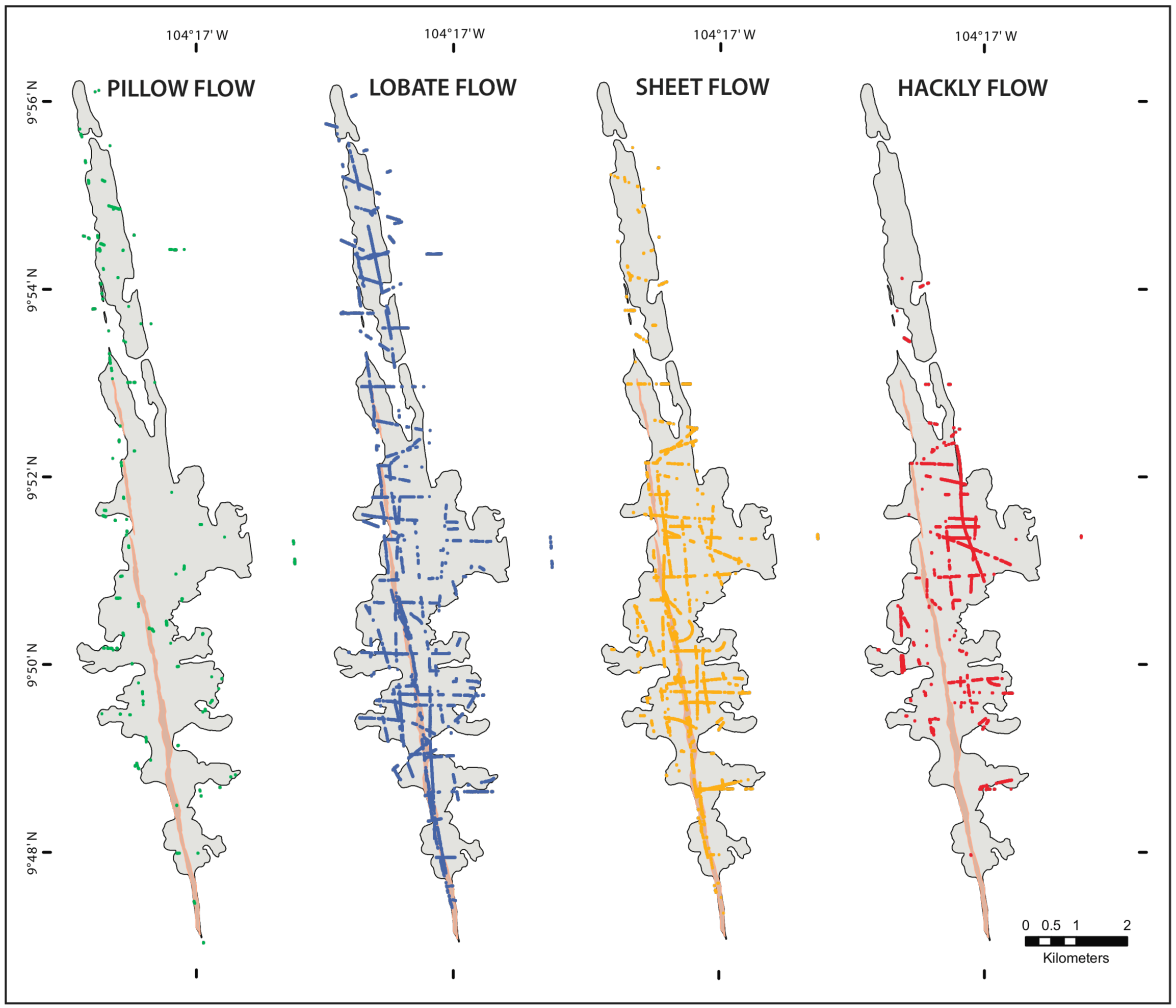

Figure 3-3. Maps showing the distribution of the four main types of morphology of the 2005–06 eruption surveyed with the TowCam. Each point represents an analyzed image and the presence of that specific morphology type.

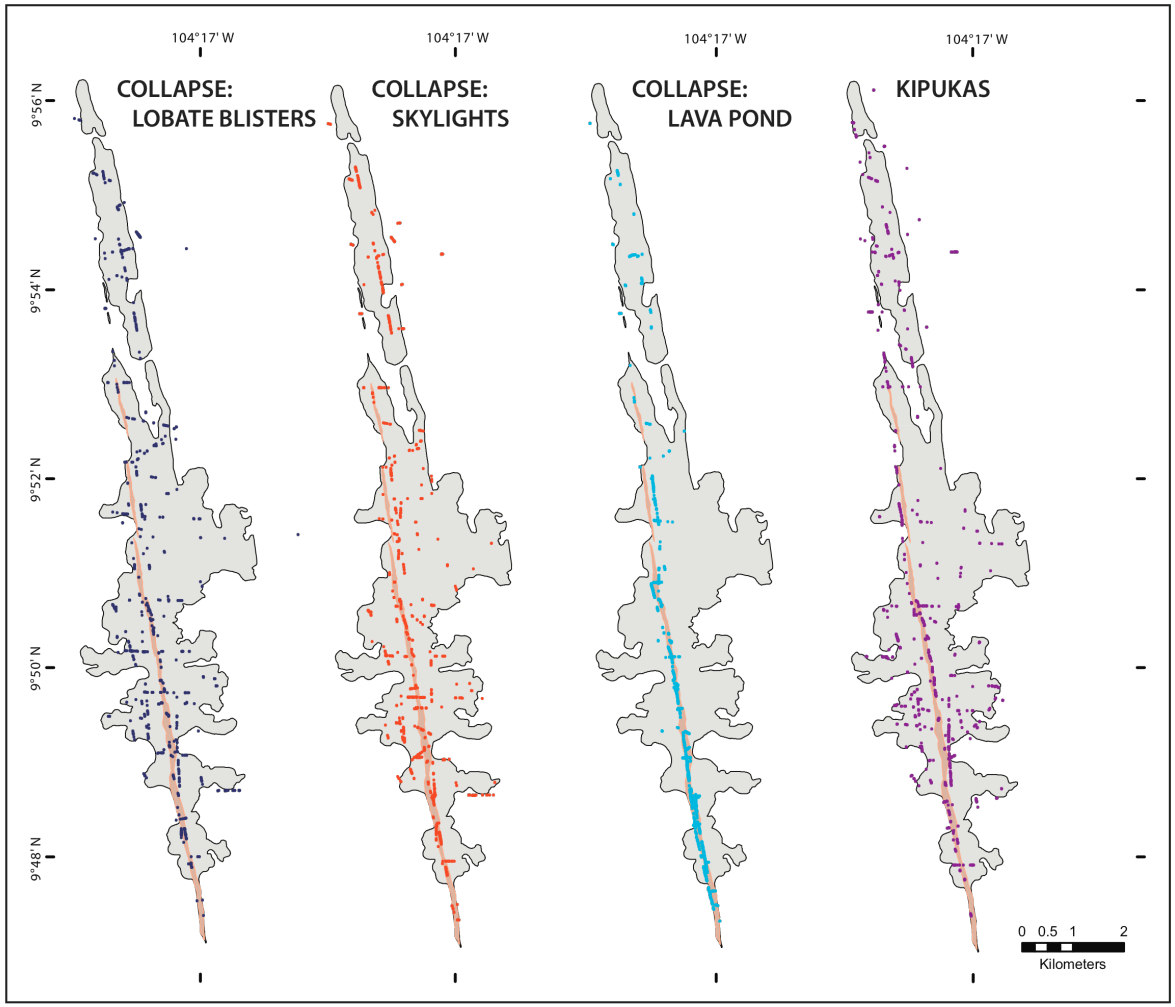

Figure 3-4. Maps show the distribution of the three size classes of collapse and kipukas. Lobate blister collapse is collapse <2 m in diameter, skylight collapse is ~2–10 m in diameter and lava pond collapse is > 10 m in diameter. Kipukas range from ~1–6 m in diameter.

CHAPTER 4
RESULTS

Abundance of Lava Morphologies

Lobate flows are the dominant lava morphology type observed in the 2005–06 flows, accounting for 52% (13,106 images) of the survey area. Sheet flows comprise 31% (7807 images) of the observed morphologies, hackly flows account for 15% (3636 images) and pillow flows account for only 2% (552 images) of the survey area. Relative to the other three morphology types, lobate flows are ubiquitous over the surveyed area but are the dominant morphology in the northern and southern regions of the flow away from of the 9°51′N lobe (Figure 4-1). Sheet flows are the dominant flow type flooring the AST and within flow channels produced by the 2005–06 eruption outside of the AST. Over 60% of pillow flows in the surveyed area are located within 100 m of the mapped flow boundary; 87% of pillows in the imagery are located within 200 m of the flow boundary (Figure 4-2). Relative to the rest of the flow, pillows are more abundant at the northern and southernmost distal ends of the 2005–06 flows (Figure 4-1).

Morphological Transitions

By examining the transitions between the different surface morphologies with respect to the AST, we can further constrain the genetic relationship between the various surface flow morphologies. There are two main types of morphological transitions seen within the 2005–06 flow: 1) gradational due to changing flow conditions, and 2) superposition of separate flows. The gradational transitions are observed between sheet and lobate flows, sheet and hackly flows, lobate and pillow flows, and lobate and hackly flows (Figure 4-3a-c). Transitions between sheet and lobate lavas vary with respect to the length scales over which they occur. Typically, they occurred over a few meters as the sheet flow develops a more lobed surface. In other cases,

where lobate flow appears to have transitioned into sheet flow, the transitions are more abrupt. The sheet flow in these cases appears to have flowed out from underneath the cooled lobate surface and is characterized by lineations that likely formed from being raked against the partially cooled upper surface [*Chadwick et al.*, 1999].

Transitions between sheet and hackly flows also vary with respect to the length scales over which they occur. In many cases, sheet flows transitioned to a jumbled flow where the sheet surface is characterized by small surface folds as the partially cooled surface deforms due continued flow of the underlying molten lava. These jumbled flows commonly transitioned into hackly flows as the flow folded surface continues to deform as it cools, ultimately breaking the surface crust. The gradation from sheet to hackly flows in these cases typically occurred over distances of 1–10 m. Sudden transitions between sheet and hackly flows, with no intermediate jumbled surface morphology, were also observed, and may reflect superposition of lavas erupted at different times.

Transitions between lobate and pillow lavas occurred over lengths <1 m, tend to occur towards the flow front termini, and are characterized by one to a few pillows branching out of well-defined lobate flows. Lobate flows near these transitions are more decorated and have distinct lobes that are minimally coalesced. The final type of gradational transition we observed is between lobate and hackly flows. These are similar to the abrupt transitions between sheet and hackly flows, where the flow surface abruptly changes character to a morphology representative of a higher rate of shear. These transitions tend to occur in association with the margins of lava channels, similar to results described by *Soule et al.* [2005].

One of the questions we intended to address through this study was whether or not individual flow fronts or pulses from the 2005–06 eruption can be identified within the interior

of the flow. There are only 5 images from the TowCam surveys where potential superposition contacts were observed within the 2005–06 flow. In these images, the morphologies do not appear to be transitioning from one type to another; rather it appears that a flow of one morphological type partially covered a flow of another flow morphology. For example, Figure 4-3d shows a lobate flow that appears to have flowed over a lineated sheet flow, both of which have been identified as 2005–06 flows using the criteria we established for our image analysis.

We used TowCam survey segments that were run perpendicular to the AST and that surveyed known lava channels to interpret the morphological evolution of a given lava flow as it moved away from an eruptive source, and to test whether the variations in distribution we see between the various morphology transitions occurred along individual flow pathways with increasing distance from the eruptive fissure. Although individual flows are occasionally characterized by lobate flows at the flow front rather than pillow lavas, the general trend is that lava morphologies associated with higher flow rates (i.e., sheet, hackly and flat-lying lobate flows) occurred near the eruptive source and transition into morphologies that are typically associated with lower flow rates towards the termini of the flow. TowCam survey AT15-6:CT06 (Figure A-2), conducted perpendicular to the axis at ~9˚51.5´N, provides an example of this transition. The images from this camera tow show that the lava emplaced closest to the axis is a mixture of sheet and hackly flows which have no clear contacts, but rather which transition from one to the other over sub-meter length scales. Further from the axis, the sheet and hackly flows transition into dominantly lobate flows, and eventually into pillow flow at the termini of the flow front. Similar relations and transitions are seen throughout the surveys (see Appendix for examples).

Distribution of Volcanic Structures

Collapse Pits

Collapse pits are a common features of submarine lava flows at fast and superfast spreading MORs that form from flow inflation and post-eruption drainback of lava [*Fornari et al*, 1998], or from a pressure gradient created along the upper crust of the flow due to the entrapment of seawater and formation of vapor [*Engels et al*, 2003; *Perfit et al.,* 2003; *Soule et al*., 2006]. As described in previous studies, these features are depressions where 2–10 cm thick surface crusts have collapsed, revealing cavities beneath [e.g., *Ballard et al*., 1979; *Sinton et al*., 2002; *Engels et al.*, 2003; *Perfit et al*, 2003; *Fornari et al.*, 2004]. In this study, collapse pits cover 19.2% (4817 images) of the total surveyed area.

Lobate blisters, collapse pits that typically occur in individual lobate lobes, account for 17.8% of the overall collapse. The larger skylights represent 27% of the overall collapse. *Engels et al.* [2003] found that lobate blisters were relatively evenly distributed within ~300 m from the AST, with only a slightly higher frequency near the ridge axis. They also reported that the distributions of skylight and lava pond collapse peak dramatically within ~100 m from the AST margin. The results we present here are similar since the distribution of both lobate blisters and skylight collapse generally decrease with increasing distance from the AST. However, in this study, the distribution of lobate blisters in addition to skylight collapse peaks within ~200 m of the AST (Figure 4-4). While there is significant difference in the distribution of collapse across the AST, there is only a slight difference in the distribution of collapse pits along the AST. In the southern extent of the main flow unit between 9°49′ and 9°48′N, there is an increase in the percent collapse observed relative to the total number of observations (Figure 4-1).

Lava pond collapse imaged in this study covers 9.8% (2659 images) of the survey area. The primary mechanism responsible for creating this extensive collapse is post-eruption

drainback of lava into primary eruptive fissures [*Fornari et al*., 1998]. Therefore, as expected, lava pond collapse imaged in this study is almost completely concentrated within the AST where erupted lava ponds within the walls of the trough (Figure 3-4).

In ~90% of the images, collapse occurred in lobate flows and the rest occurred in sheet flows, which is consistent with results reported by *Engels et al.* [2003]. In the images from the camera surveys used in this study, it is apparent that these networks of interconnected collapse areas play a role in the transport of lava during eruptions [*e.g.*, *Haymon et al.,* 1993; *Shouten et al*., 2002; *Fornari et al.*, 1998, 2004]. We see evidence that subsurface pathways were exploited by 2005–06 flows, with new lava imaged at the base of collapse pits located in older flows (Figure 4-5a). We also observe areas of older lava crust, broken and lying on the surface of the 2005–06 flows, that was presumably pushed up by lava flowing within these subsurface networks (Figure 4-5b).

Vapor formed by lava-seawater interactions [*Perfit et al.*, 2003; *Soule et al.*, 2006] also seems to have played a significant role in the development of these extensive areas of collapsed lobate consistent with observations of *Engels et al.* [2003]. Features within the crust of sheet and hackly flows also suggest the presence of vapor in their development (Figure 4-6).

Kipukas

Kipukas <6 m in diameter were seen in 4.3% (1170 images) of the survey images. These areas of older lavas exposed through the new flows indicate that the flow is ~1–2 m thick [*Soule et al*., 2007a]; kipukas are associated with lobate forms in 88% of the observations, pillow forms in 9%, sheet flows in 3%, and hackly flows in <1% of the observations. These small kipukas are typically individual lobes of sheet flow or lobate flows that divert and wrap around areas of older flow. Kipukas commonly occur where there is no clear topographic barrier, or where there is an increase in seafloor roughness often when pillows or inflated lobate lavas characterize the pre-

eruption surface. Although, kipukas are found throughout the survey area, they are mostly concentrated in the northern and southern regions of the flow area, following similar trends to the distribution of lobate and pillow flows. Additionally, kipukas are correlated with proximity to flow boundaries (Figure 4-2).

Faults and Fissures

Only one fault north of 9°52′N, against which the 2005–06 flow dammed [*Soule et al.*, 2007a], and 14 fissures were seen in the survey images. The imaged fissures are associated with the AST or with the off-axis fissures north of 9°52′N. *Escartin et al.* [2007] noted that volcanism at MORs, and the fast-spreading EPR specifically, efficiently buries faults within 2 km of the axis. Thus, the lack of faulting we see within the 2005–06 flow, which is predominately within 2 km of the axis, is consistent with what we would expect for recently repaved seafloor, and consistent with studies of the same area prior to the eruption [*Fornari et al.*, 2004; *Escartin et al*., 2007].

Sidescan Sonar Imagery

One of the limitations inherent in seafloor photography surveys is the amount of area that can be surveyed by the images. In order to interpret the 2005–06 flows beyond the scope of the camera surveys, we use data from the TowCam surveys to ground truth the sidescan imagery collected in 2007. This allows for the correlation of specific morphologies with the variable acoustic patterns observed in the sidescan imagery. However, it is not always possible to directly correlate the sidescan imagery and the images from the camera surveys due to differences in the navigational precision between the two data sets and the short length scales over which changes in flow morphology occur. Here, we use images from camera surveys that utilized the most precise navigation method (LBL) to interpret an area of the sidescan imagery where confidence in the navigational precision was highest (Figure 4-7).

Because there is only a thin layer of sediment on the EPR crest, and virtually no sediment on the newly erupted lava flows, there is little absorption of sound energy, and hence the acoustic texture in the sidescan imagery is most influenced by the slope and roughness of the volcanic seafloor [e.g., *Blondell and Murton*, 1977; *Scheirer et al.,* 2000; *Escartin et al.,* 2007; *Meyer and White*, 2007]. The most prominent features seen in the sidescan imagery are sinuous areas of low backscatter intensity that represent lava channels comprised of smooth sheet flows emanating from the AST [e.g., *Soule et al*, 2005]. The 9˚51´N lobe contains the longest of these lava channels, emplaced as far as 3 km off axis, supporting the idea that these channels serve as distribution pathways for erupted lava [*Soule et al.* 2005, 2007a]. Interspersed between these channels floored by sheet flows are rough, hackly flows that are characterized by highly specular acoustic textures (brighter areas in the sidescan imagery). The smooth-to-mottled areas of medium backscatter intensity are interpreted to be lobate or pillow lavas with relatively low relief and roughness intermediate to sheets and pillows. The sidescan imagery shows the outward convex acoustic patterns, indicative of flow fronts along the ridge crest common to fast and superfast spreading ridges [*Sinton et al.*, 2002; *Fornari et al*., 2004; *Soule et al.*, 2007a]. Camera survey images reveal that these regions are characterized by lobate and pillow flows, and therefore potentially mark the termini of flow fronts. However, it is difficult to determine if these flow fronts were produced by the 2005–06 flows or if they are pre-existing flow fronts covered by a thin veneer of the 2005–06 flows. In some places, the textures are clearly different between the pre- and post-eruption sidescan imagery; in others it appears that the flow fronts may still be there, but are subdued, which may indicate the flow went over the pre-existing front and draped it, but did not obliterate its relief. The latter is an indication of how thin the 2005–06 flows are, estimated to be ~1–2 m thick [*Soule et al*., 2007a].

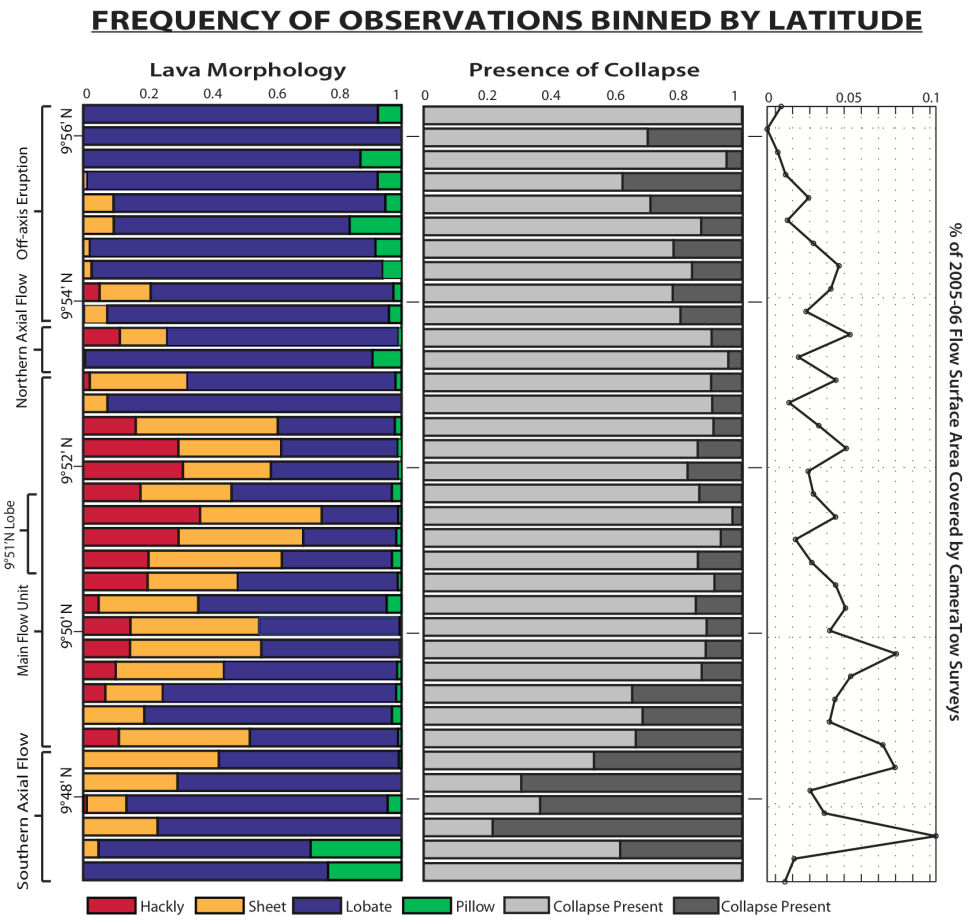

Figure 4-1. Observations of morphology type and presence of collapse binned by 500 m of latitude. The percent of the 2005–06 flow surface area covered by the surveys was calculated by assuming the pictures covered an area of ~23 m^2.

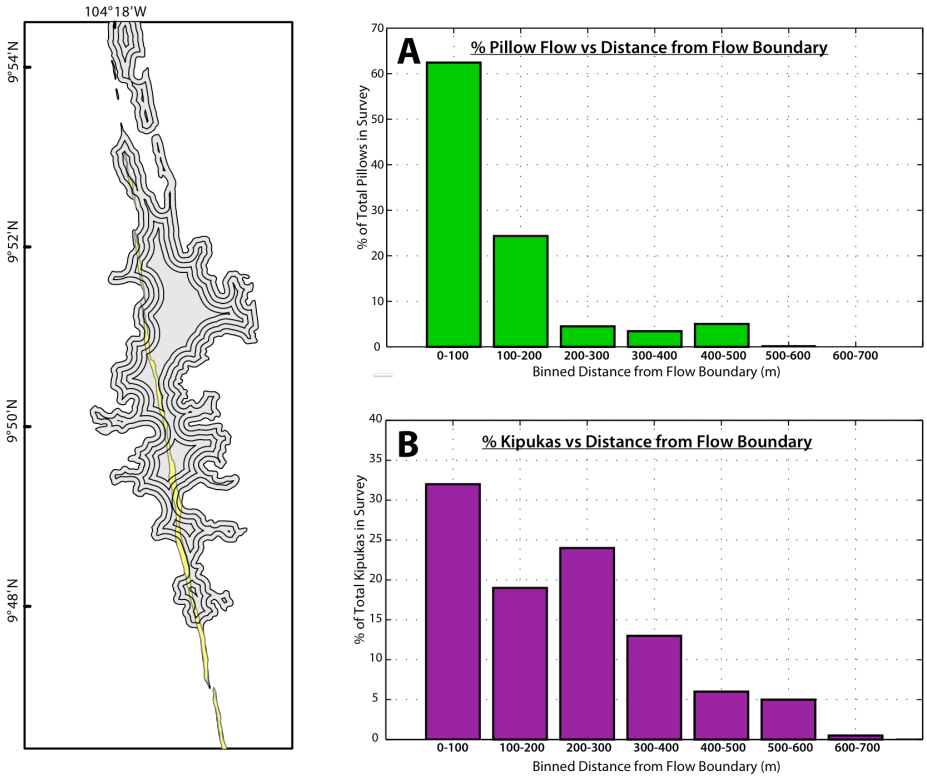

Figure 4-2. Map showing the location of 100 m bins relative to the flow boundary. A) >60% of pillow flows are within 100 m of the mapped flow boundary and >87% occur within 200 m, indicating that pillows formed from slow effusion rate and decreased lava supply at the flow margins. B) Kipukas are also correlated with proximity to the flow boundary.

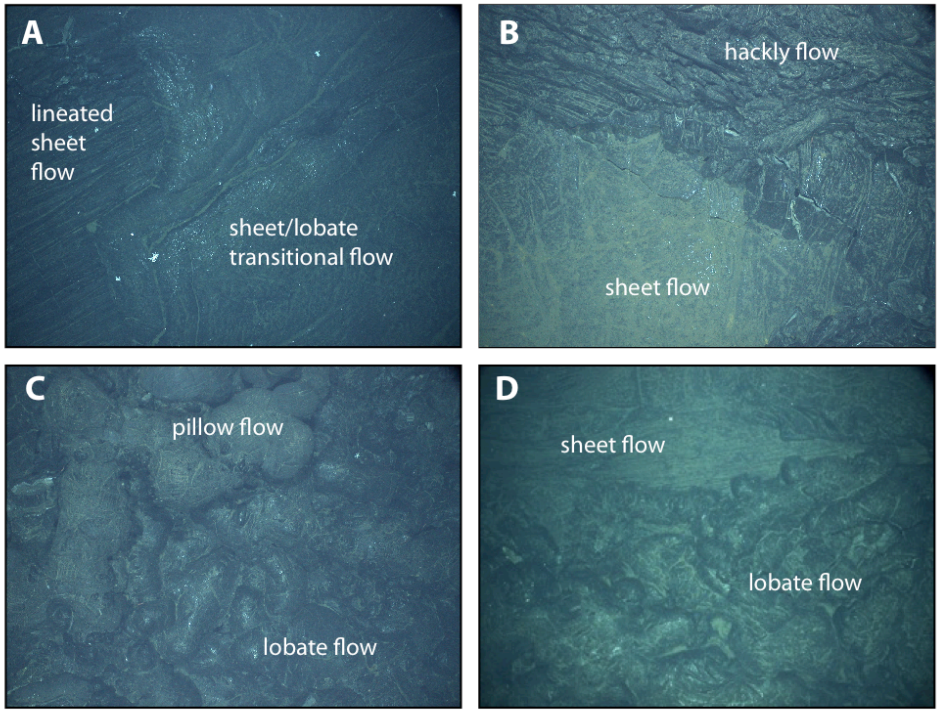

Figure 4-3. Examples of transitions between different morphologies of the 2005–06 flow. A) A sheet/lobate transitional morphology abruptly transitioning into a lineated sheet flow (~6 m x 4.5 m). B) A sheet flow abruptly transitioning into hackly flow (~4.8 x 3.6 m). C) Pillow flow developing towards a flow front (~4.8 m x 3.6 m). D) A potential example of superposition where a lobate flow appears to have flowed over a lineated sheet flow (~7 m x 5.3 m).

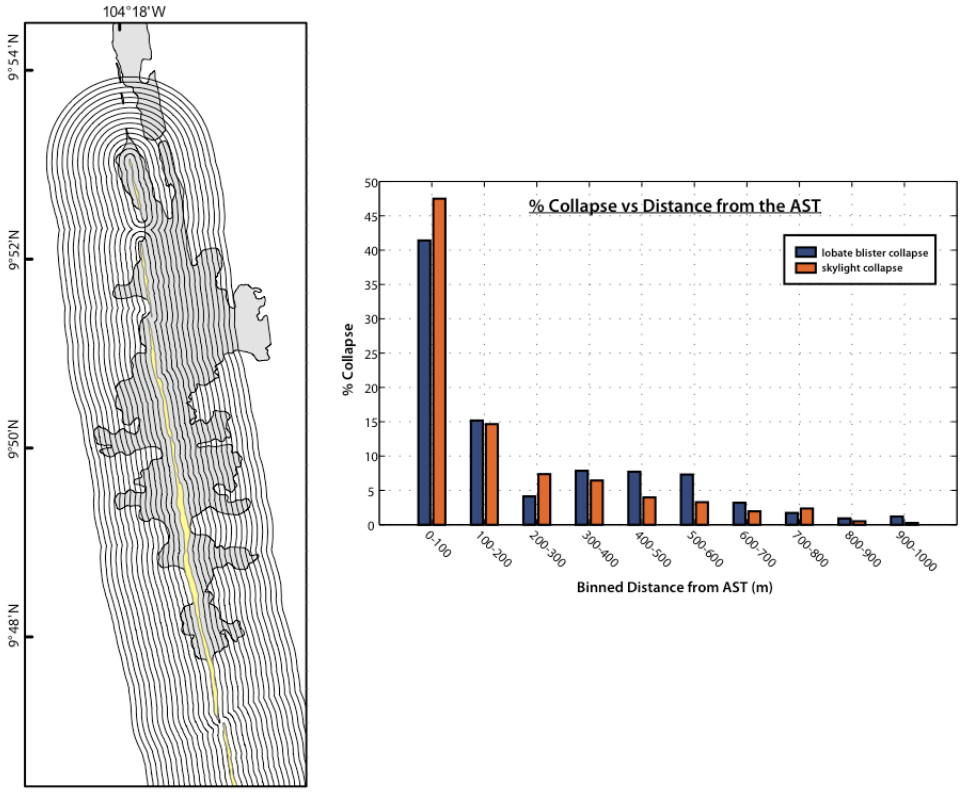

Figure 4-4. Map showing the location of 100 m bins relative to the AST. The distribution of collapse <2 m in diameter (lobate blisters) and collapse ~2–10 m in diameter (skylight collapse) are similar relative to distance from the AST. Collapse is primarily concentrated within 100 m of the AST.

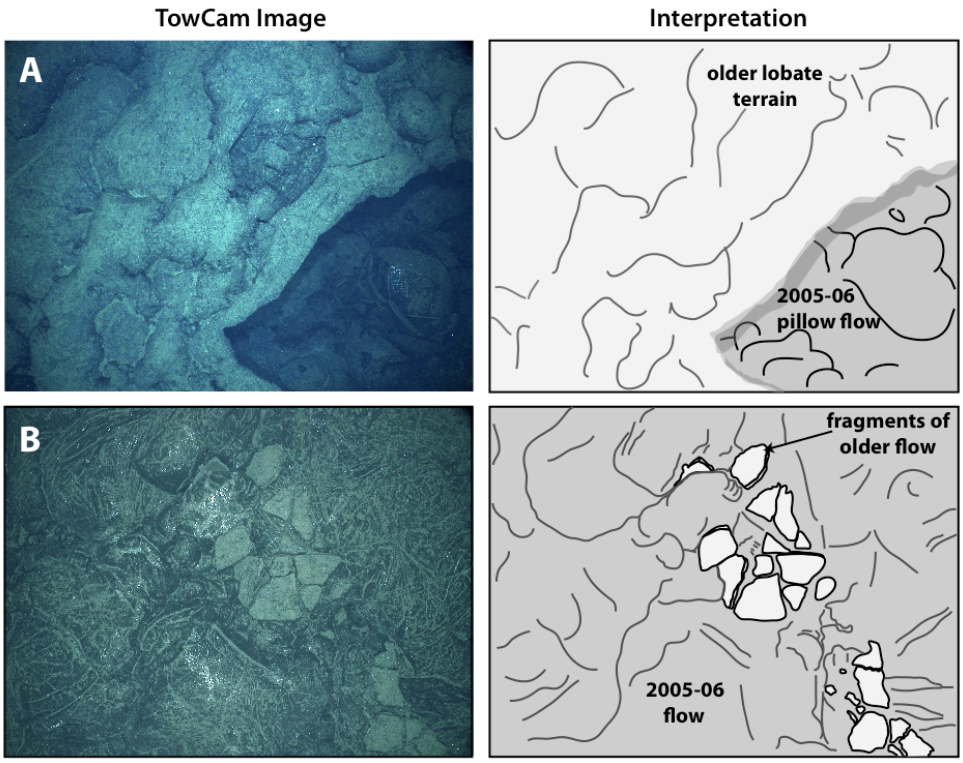

Figure 4-5. Evidence that subsurface pathways were utilized by the 2005–06 flows. A) 2005–06 pillow lava imaged at the base of collapse in older lobate terrain (~6 m x 4.5 m). B) Older lava crust broken and lying on the surface of the 2005–06 flow that was presumably pushed up by lava flowing within subsurface networks (~4.8 m x 3.6 m).

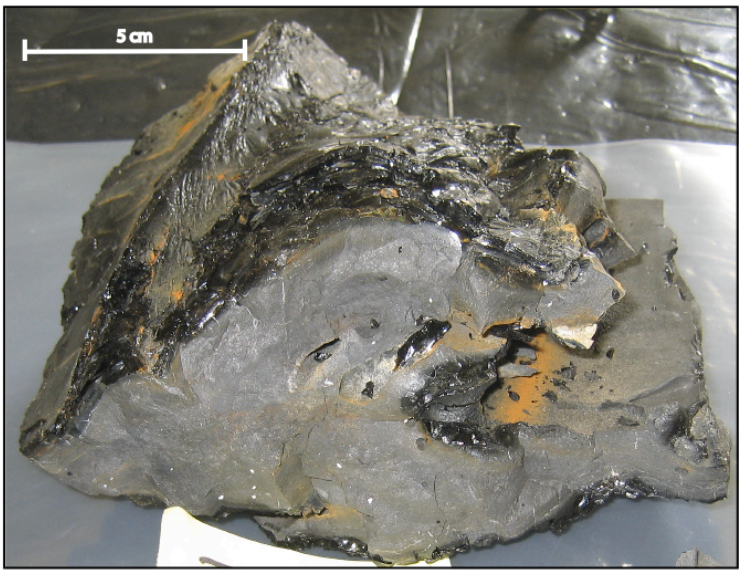

Figure 4-6. Cross-sectional view of a 2005–06 EPR hackly flow showing thick outer glass rind and open cavities (some with glass and some without) within the interior of the rock and in the core of the central fold. Non-glassy textures of the cavities are similar to those observed on the undersides of collapsed lobate flows suggesting they formed by lava-vapor interactions. Subsequently the flow was intensely deformed before it completely solidified but preserving the earlier formed surface textures.

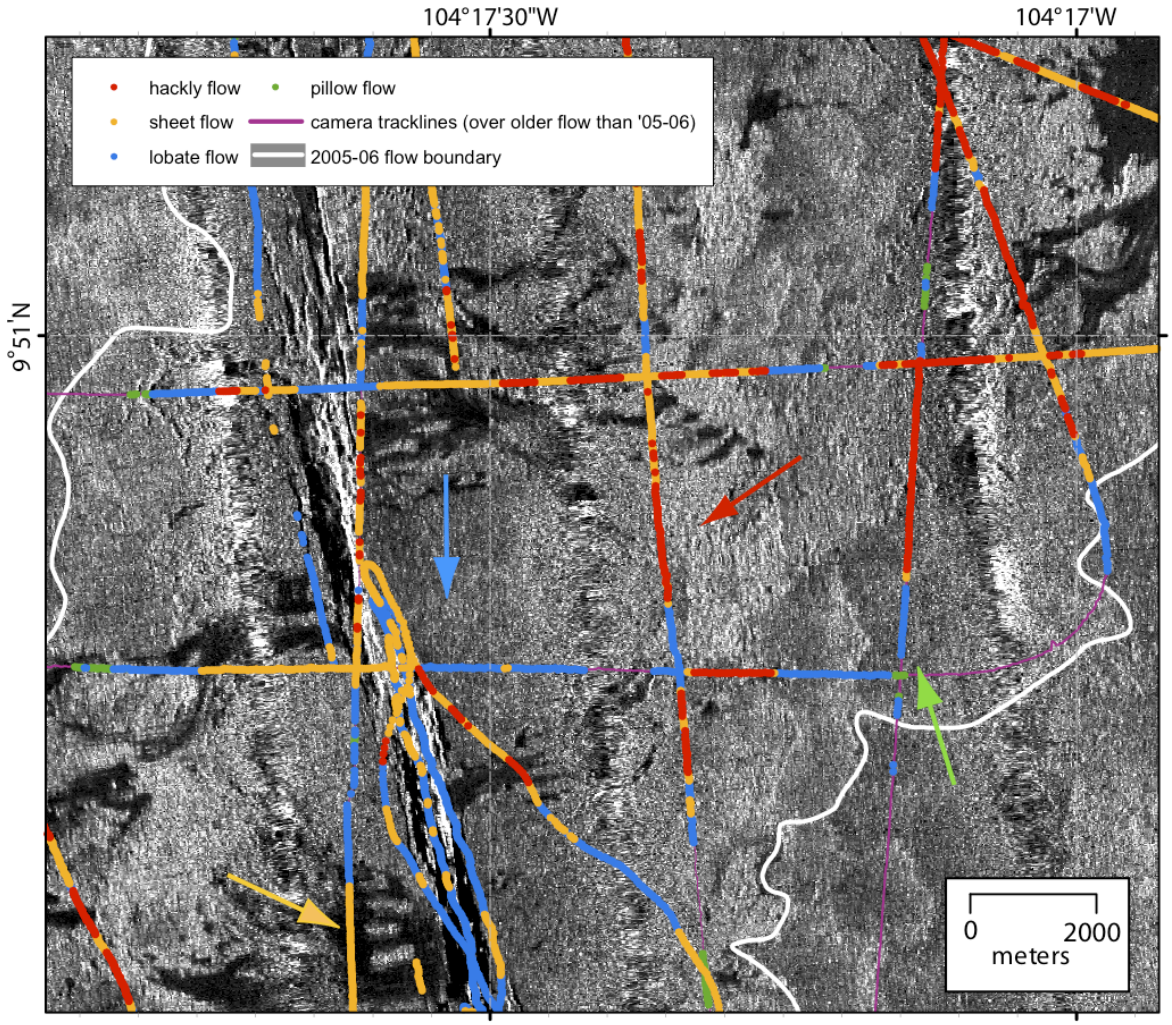

Figure 4-7. Sidescan sonar imagery collected in 2007 overlain with observations from TowCam surveys. Location of the map area is represented by the dashed white box on Figure 1-1. The yellow arrow points to an area of low backscatter intensity representing lava channels comprised of smooth sheet flows emanating from the AST. The blue arrow points to a medium backscatter intensity mottled area representative of the texture we interpret to be lobate flows. The red arrow points to a highly specular acoustic texture that we interpret to be hackly flows. The green arrow points to an outwardly convex acoustic pattern indicative of a flow front of pillow and/or lobate flows.

CHAPTER 5
DISCUSSION

In this study, we used lava surface morphology as an indicator of relative effusion and flow rates for the 2005–06 flows. Previous studies have suggested a variety of intrinsic and extrinsic parameters, in addition to effusion rate, that may influence the development of distinct flow morphologies including: lava rheology (i.e., composition, temperature, and crystallinity), the pre-existing slope and terrain, and local slope angle [e.g*., Bonatti et al.,* 1988; *Rowland and Walker*, 1990; *Griffiths et al*., 1992; *Gregg and Fink*, 1995; *Gregg et al*., 1996]. We show below the pre-existing slope and terrain did not significantly affect the morphology of the 2005–06 flows. Additionally, petrologic and geochemical analyses of volcanic glass samples suggest that the flow rheology remained relatively constant throughout the course of the eruption. Samples from the 2005–06 flows are relatively homogeneous compositionally and are mostly aphyric (<5% plagioclase and olivine) [*Soule et* al., 2007a; *Goss et al*., in review]. Thus, effusion and local flow rates remain the key controls on surface morphology of the 2005–06 flows. Using the empirical relationship between flow rate and morphology, we conclude that the 2005–06 event erupted at higher rates than previously estimated for the 1991–92 eruption. Additionally, the 2005–06 event was most voluminous, and flow rates were highest, within the 9˚51´N flow lobe, further suggesting that this was the primary locus of the diking event that fed the eruption.

Influence of Pre-existing Slope and Terrain on Surface Morphology

The EPR at ~9°50′N has been studied for ~20 years by near-bottom imaging [e.g., *Haymon et al*., 1991; *Kurras et al*., 2000], providing a substantial volume of data that can be used to assess changes caused by seafloor eruptions, and to infer the processes responsible for creating the lava flow surface morphologies. To assess whether the pre-eruptive surface influenced the extent and morphology of the 2005–06 eruptions, information collected from the

recent TowCam surveys was augmented by four studies of the area prior to the 2005–06 eruption. These included: (1) camera-tow surveys of the terrain prior to the 2005–06 [*Kurras et al.*, 2000], (2) bathymetric data collected by WHOI's Autonomous Benthic Explorer (ABE) in 2000 [*Fornari et al*., 2004], (3) bathymetric data collected by the 30 kHz EM300 multibeam system in November of 2005 [*White et al.*, 2006], and (4) sidescan sonar data collected in 2001 [*Fornari et al.*, 2001, 2004; *Schouten et al.*, 2002; *White et al.*, 2002; *Escartin et al*., 2007].

Kurras et al. [2000] analyzed camera-tow surveys collected along and across the axis of the EPR prior to the 2005–06 eruption. Four of these deep-towed camera survey lines traversed areas that were subsequently covered by the 2005–06 flows, and were conducted in areas in close proximity to post-eruption survey lines. The pre-eruption surveys were reanalyzed using the classification scheme we adopted, and used in conjunction with pre-eruption sidescan sonar data [*Fornari et al.*, 2004] to investigate whether the morphology of the pre-existing terrain influenced the morphology produced during the recent eruption. EM300 multibeam bathymetry data [*White et al.*, 2006] and ABE Imagenex 120 kHz scanning altimeter bathymetry data collected in 2000 by ABE [*Fornari et al*., 2004] were used to determine the pre-existing slope of the terrain prior to the 2005–06 flows [e.g., *Gregg et al.*, 1996]. The EM300 survey covered the entirety of the area subsequently covered by the 2005–06 flow; however, it is gridded at a lower resolution than the ABE survey, which covered a smaller area at 9°50´N. The local pre-existing slope surrounding each image location was derived from the 30 m x 50 m gridded EM300 depth measurements and 5 m x 5 m gridded ABE depth measurements by calculating the average gradient of the four nearest grid cells at each image position, to account for uncertainties in navigation.

Pre-existing Slope Analysis

We derived slopes of ~0˚–11˚ from the EM300 bathymetry and ~0˚–19˚ from the ABE bathymetry within the area of the new flows. Analysis of lava morphology as a function of topographic slope derived from both gridded depth determinations indicates that all four lava morphologies can be found over the entire range of slopes within the flow (Figure 5-1), suggesting that the pre-existing slope was not a controlling factor of the 2005–06 flow surface morphology. As a further check on whether slope correlates with seafloor morphological variations, we analyzed lava morphology as a function of topographic slope derived from near-bottom TowCam depth profiles (Appendix). Our analyses indicate that there is no correlation between topography created by the 2005–06 flow and the resulting lava morphology.

Pre-existing Morphology Analysis

The four TowCam surveys used in this study conducted prior to the 2005–06 flows were analyzed in areas where they overlapped the mapped 2005–06 flow boundary (Figure 5-2). These morphology observations were compared to morphologies of the 2005–06 flow that are located within 100 m of the pre-eruption surveys. The 100 m buffer accounts for navigational uncertainties in the layback calculations. In the 1997 surveys, lobate lavas were ubiquitous over the area surveyed and accounted for 74% of the observed morphologies. Hackly lavas comprised 11% of the morphologies observed, sheet lava was less abundant comprising only 8% of the morphologies in the surveyed area, and 7% of the lava was pillow. Areas that were predominately lobate in the 2005–06 main flow lobe prior to the recent eruptions were overprinted by sheet and hackly flows during the 2005–06 eruption. The post-eruption surveys indicate that, within the 100 m buffer zone of the pre-eruption surveys, the abundance of lobate, sheet, and hackly morphologies changed significantly over the span of two eruption cycles. In recent surveys, lobate lava was seen much less than in the pre-eruption surveys, accounting for

only 34% of the morphologies observed. Sheet flows are currently the dominant morphology type observed, accounting for 65% of the morphologies within the study area, 34% of which are hackly and 31% lineated or ropey sheet. Only 1% of the morphologies observed are pillow. The results of this comparison indicate that the pre-eruption morphology was not a dominant controlling factor in determining the morphology of the 2005–06 eruption.

Evidence of High Eruption Rates for the 2005–06 Eruption

The comparison of the pre- and post-eruption morphologies indicates the effusion rates differed considerably within the 9˚51´N lobe between the 2005–06 and the 1991–92 eruptions. The substantial increase in the presence of sheet and hackly flows and presence of new lava channels that fed these flows over the span of the two eruptions supports the idea that the 2005–06 event erupted with a higher effusion rate than what is typical for this fast-spreading MOR [*Soule et al.*, 2007a].

The abundance and distribution of collapse within the 2005–06 flows are also consistent with higher than typical eruption rates for this region of the EPR. Collapse occurred throughout the 2005–06 flows, however it occurred with a significantly higher frequency within 100 m of the AST and almost exclusively within lobate flows. While our conclusion that collapse typically occurred within lobate terrain agrees with that of Engels et al. [2003], we note a difference in that collapse within the 2005–06 flows peaks within 100 m of the AST, rather than being more evenly distributed across the EPR crestal plateau as observed by Engels et al. [2003]. The formation of collapse has been hypothesized to occur from the withdrawal of lava back into eruptive fissures or into the network of tube and channel systems in the subsurface of the ridge flanks [*Haymon et al.* 1993; *Fornari et al.*, 1998] or alternatively, from a pressure gradient created by cooling vapor pockets underlying the upper crust of the lava flow [*Engels et al.*, 2003; *Perfit et al.,* 2003]. In either case, the greater abundance of collapse near the eruptive vent leads

us to the conclude that eruption rates for the 2005–06 flows were higher than previous eruptions in the same area. Higher eruption rates would result in a greater accumulation of lava near the vent (and across a wider area) that – as eruption rates waned – would drain both downflow and into eruptive fissures, promoting collapse. In addition, higher eruption rates might promote the incorporation of greater amounts of seawater into the active flow, thereby facilitating an increase in collapse.

Eruption Length and Distribution of Morphology Along Axis

The volume of lava erupted during the 2005–06 event varied substantially along the ~18 km long eruptive fissure system. In some locations, the terminating flow front is located < 0.5 km from the AST, while in other locations flow lobes extend as far as ~3 km from the AST. The most voluminous output of the 2005–06 eruption occurred within the 9˚51´N lobe, coincident with the highest density of active high-temperature hydrothermal venting [*Fornari et al., 2004*], slight geochemical segmentation [*Goss et al*., in review], and discontinuities in the underlying axial magma chamber [*Carbotte et al.*, 2009]. Relative to the rest of the flow, this region contains the highest percentage of high-flow rate morphologies (~70% sheet and hackly flows) and is where lava was transported farthest from the AST. The 9˚51´N lobe likely coincides with the most active fissure segment within the AST and is the inferred site of the primary diking event that fed the 2005–06 eruption [*Tolstoy et al*., 2006]. However, this region is not the only place that experienced higher eruption rates than those of the 1991–92 eruption. While the 9˚51´N lobe experienced the most voluminous and highest abundance of high-effusion flows, based on interpretations of sidescan imagery of the pre- and post-eruption terrain and our image analyses, we see an increase in sheet and hackly flows within almost all of the 2005–06 flow lobes. We conclude from these observations that the entire length of the axial eruption

experienced higher eruption rates than previous studied eruptions, but with decreased lava supply outside of the 9°51´N flow lobe.

The relative distributions of the four morphology types along axis further indicates that the most recent eruption was focused at a primary fissure within the AST at 9°51´N. While all morphologies are observed along the length of the 2005–06 main flow unit, the relative abundance of sheet and hackly flows is greatest around the 9°51´N lobe and the relative abundances of lobate and pillow flows increase with along-axis distance from this region (Figure 4-1). This observation, in conjunction with our previous analyses, indicates that flows at the northern and southern distal ends of the 2005–06 axial eruption did not have a sufficient supply of lava to produce high abundances of high-flow rate morphologies seen elsewhere through the area covered by this eruption.

Distribution of Morphology Across Axis

The formation of the four morphologies classified in this study is dependent on flow rate. The general across-axis trend that we observe in the 2005–06 flow is that axially erupted lavas formed sheet and flat-lying lobate flows near the vent and then transitioned into less coalesced lobate and pillow flows with greater distance. The majority of pillow flows imaged in the surveys (>80%) were found at the terminating flow boundaries, indicating that distal flow fronts were advancing at relatively slower rates. As the flow surface morphologies likely reflect the flow conditions at the time of solidification, this organization in morphologies suggests that flow rates were higher during the initial stages of the eruptions and waned with increasing time (i.e., distance travelled across the seafloor). The greater abundance of pillows at the margins of flow lobes should help us identify the separate pulses that comprised the 2005–06 eruption [e.g., *Rubin et al*, 2006, 2008, in prep], but there is not substantial evidence of internal pillow fronts in

the survey images. The flow fronts of the 2005–06 eruption, however, often terminate as lobate flows rather than pillow fronts, making it more difficult to distinguish these separate pulses from one another within the interior of the flow.

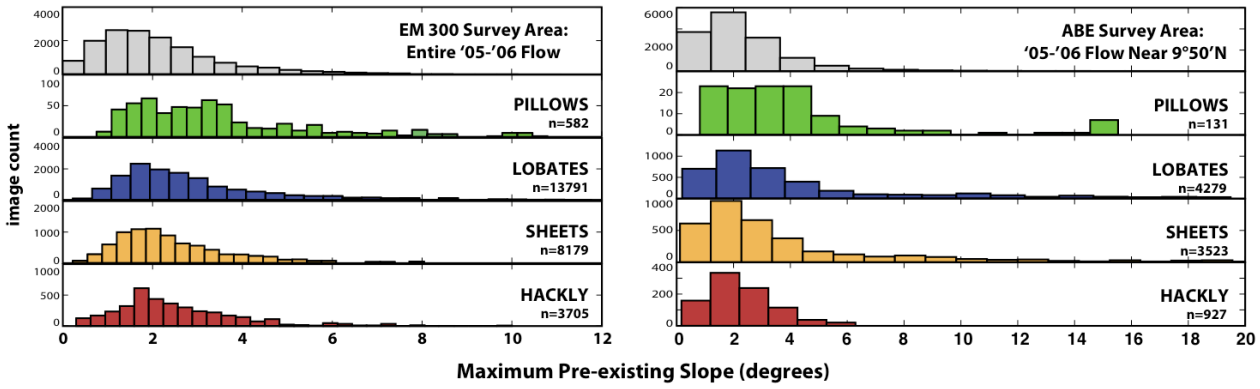

Figure 5-1. Lava morphology plotted as a function of pre-existing slope as calculated from the bathymetric surveys conducted with the EM300 multibeam system and ABE. The local pre-existing slope surrounding each image location was derived from the 30 m x 50 m gridded EM300 depth measurements and 5 m x 5 m gridded ABE depth measurements by calculating the average gradient of the four nearest grid cells at each image position to account for uncertainties in navigation. All four morphologies can be found over the entire range of pre-existing slopes, indicating pre-existing slope was not a dominant controlling factor of the 2005–06 EPR eruption surface morphology.

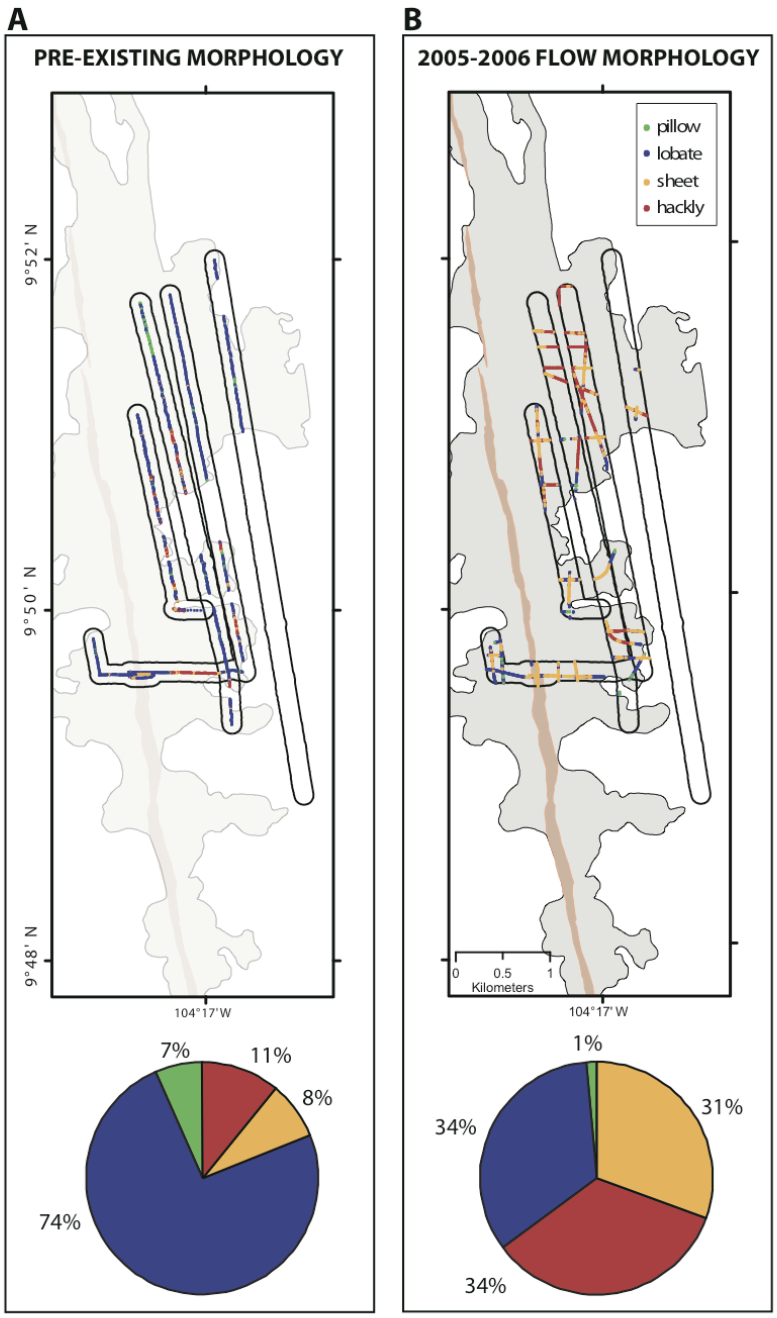

Figure 5-2. A) Pre-eruption camera surveys on the EPR crest (*Kurras et al.*, 2000) were analyzed in areas where they overlapped with the mapped 2005–06 flow. These surveys indicate that the pre-existing terrain was largely characterized by lobate flows. B) Morphology of the 2005–06 EPR flow within the same region as the pre-existing camera surveys. The black lines represent a 100 m buffer surrounding each pre-eruption survey line to account for navigational uncertainties. The percentages of sheet and hackly flows are significantly higher in the 2005–06 EPR eruption.

CHAPTER 6
CONCLUSIONS

This study provides the most comprehensive analysis of imagery data over a well-defined and mapped MOR eruption. From our analyses and interpretations of deep-towed camera surveys, high-resolution bathymetric profiles and sidescan sonar imagery, we draw the following conclusions:

- The 2005–06 eruption is characterized by 52% lobate flows, 31% sheet flows, 14% hackly flows and 2% pillow flows. Over 80% of the pillow flows occurred within 200 m of the flow boundary, indicating that pillows formed from a slowed flow rate and decreased lava supply at the flow margins. Collapse is abundant throughout the 2005–06 flows, but is primarily concentrated within 100 m of the AST. The distribution of collapse indicates that inflation and deflation processes were dominant near the vent, but occurred to greater distances than previous EPR eruptions, and/or that a greater amount of seawater was incorporated into the active flow within this region.

- The bulk of the eruption occurred within the 9˚51´N lobe, which is characterized by ~70% sheet and hackly flows indicative of high lava flux rates. Lava channels within this region served as distribution pathways that allowed the lava to travel as far as ~3 km off axis.

- Surface morphology of the 2005–06 flows was primarily controlled by effusion and lava flow rates and was not influenced by the pre-existing terrain, slope or lava rheology.

- The dynamics of the 2005–06 eruption were substantially different than those of the previous eruption in 1991–92. The increased abundance of lava channels, high-flow rate morphologies, and the distribution of volcanic collapse suggest that the most recent eruption was more voluminous and was characterized by higher eruption rates than the 1991–92 event. The entire length of the axial eruption experienced higher eruption rates, but the signal of this is most pronounced within the 9°51´N flow lobe due to a greater amount of lava supply.

APPENDIX
TOWCAM PROFILES

Figure A-1. Inset of map at left showing the position of TowCam survey lines across the 2005–06 EPR eruption. Survey profiles are color coded to flow morphologies: green represents pillow flows, blue represents lobate flows, orange represents sheet flows, and red represents hackly flows. Reference points on the map and profile are marked as A & B. The survey profiles show examples of typical across-axis morphological transitions observed in the 2005–06 EPR flows. In this recent eruption, axial erupted lavas formed sheet and lobate flows near the AST, and then transitioned into lobate and pillow flows with greater distance from the AST (see text for discussion). Slope calculations are derived from near-bottom TowCam depth profiles. All morphologies occur over the entire range of slopes, indicating that slope created by the 2005–06 EPR eruption did not influence the surface morphology.

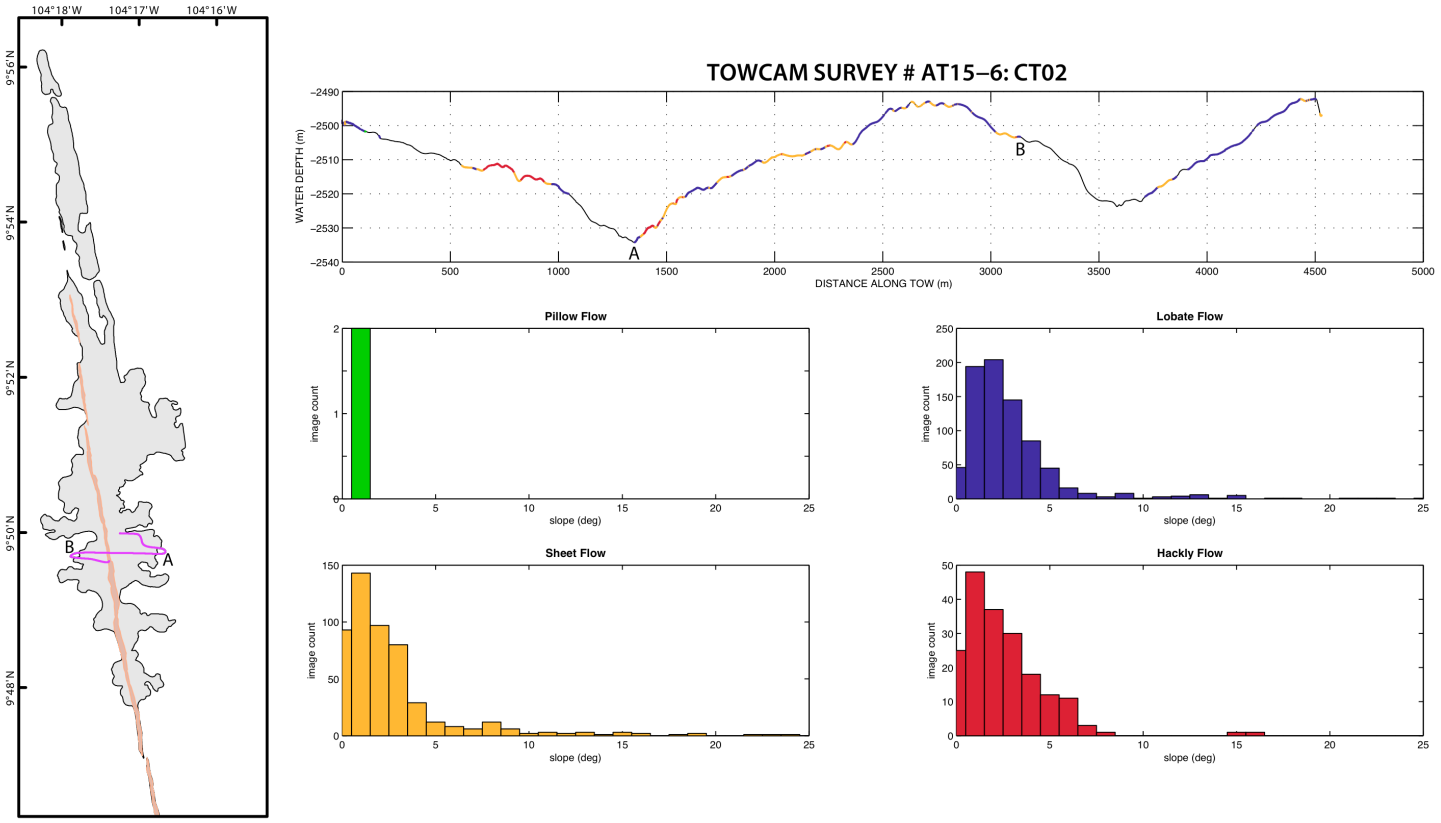

Figure A-2. Inset of map at left showing the position of TowCam survey lines across the 2005–06 EPR eruption. Survey profiles are color coded to flow morphologies: green represents pillow flows, blue represents lobate flows, orange represents sheet flows, and red represents hackly flows. Reference points on the map and profile are marked as A & B. The survey profiles show examples of typical across-axis morphological transitions observed in the 2005–06 EPR flows. In this recent eruption, axial erupted lavas formed sheet and lobate flows near the AST and then transitioned into lobate and pillow flows with greater distance from the AST (see text for discussion). Slope calculations are derived from near-bottom TowCam depth profiles. All morphologies occur over the entire range of slopes, indicating that slope created by the 2005–06 EPR eruption did not influence the surface morphology.

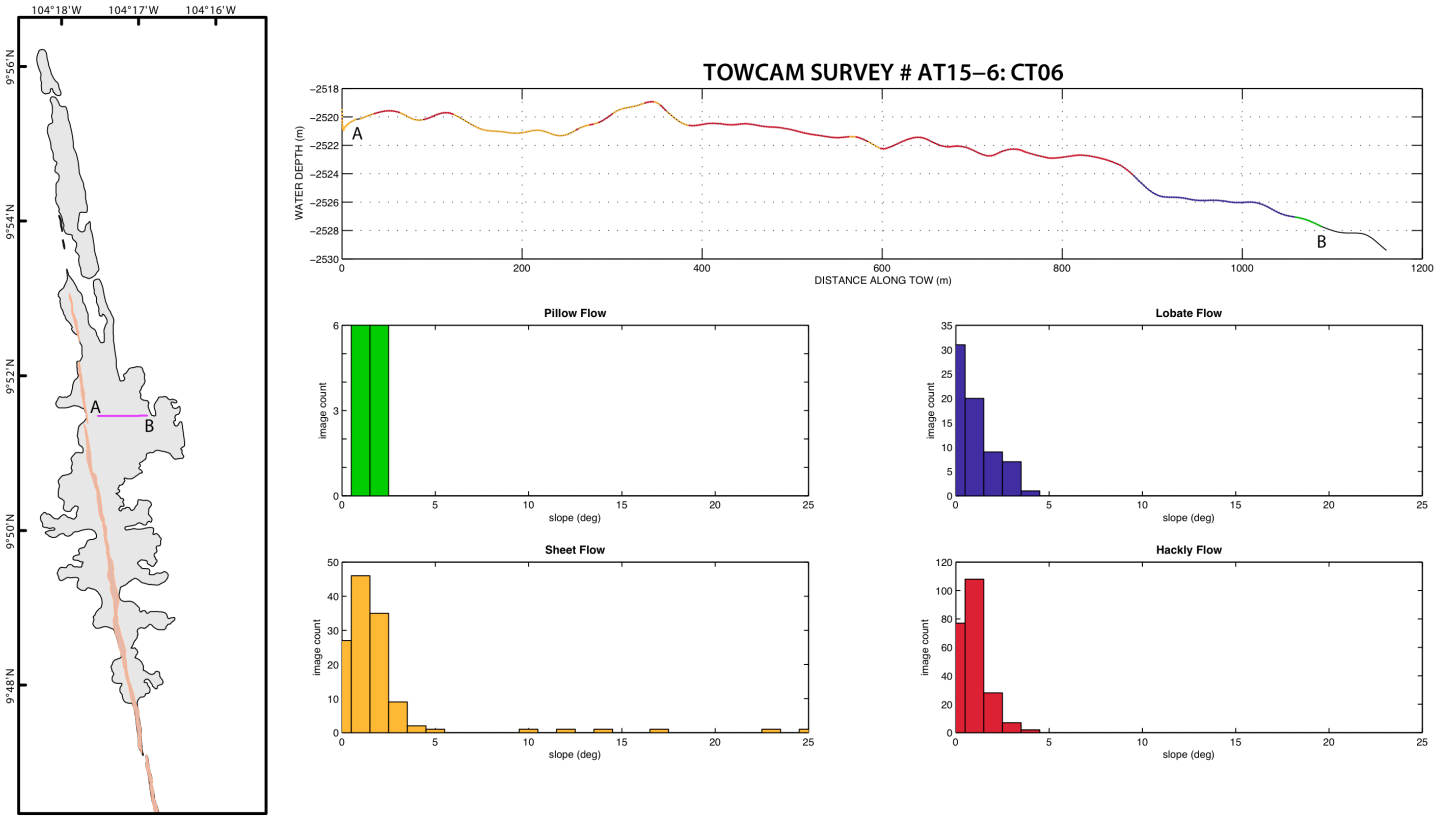

Figure A-3. Inset of map at left showing the position of TowCam survey lines across the 2005–06 EPR eruption. Survey profiles are color coded to flow morphologies: green represents pillow flows, blue represents lobate flows, orange represents sheet flows, and red represents hackly flows. Reference points on the map and profile are marked as A & B. The survey profiles show examples of typical across-axis morphological transitions observed in the 2005–06 EPR flows. In this recent eruption, axial erupted lavas formed sheet and lobate flows near the AST and then transitioned into lobate and pillow flows with greater distance from the AST (see text for discussion). Slope calculations are derived from near-bottom TowCam depth profiles. All morphologies occur over the entire range of slopes, indicating that slope created by the 2005–06 EPR eruption did not influence the surface morphology.

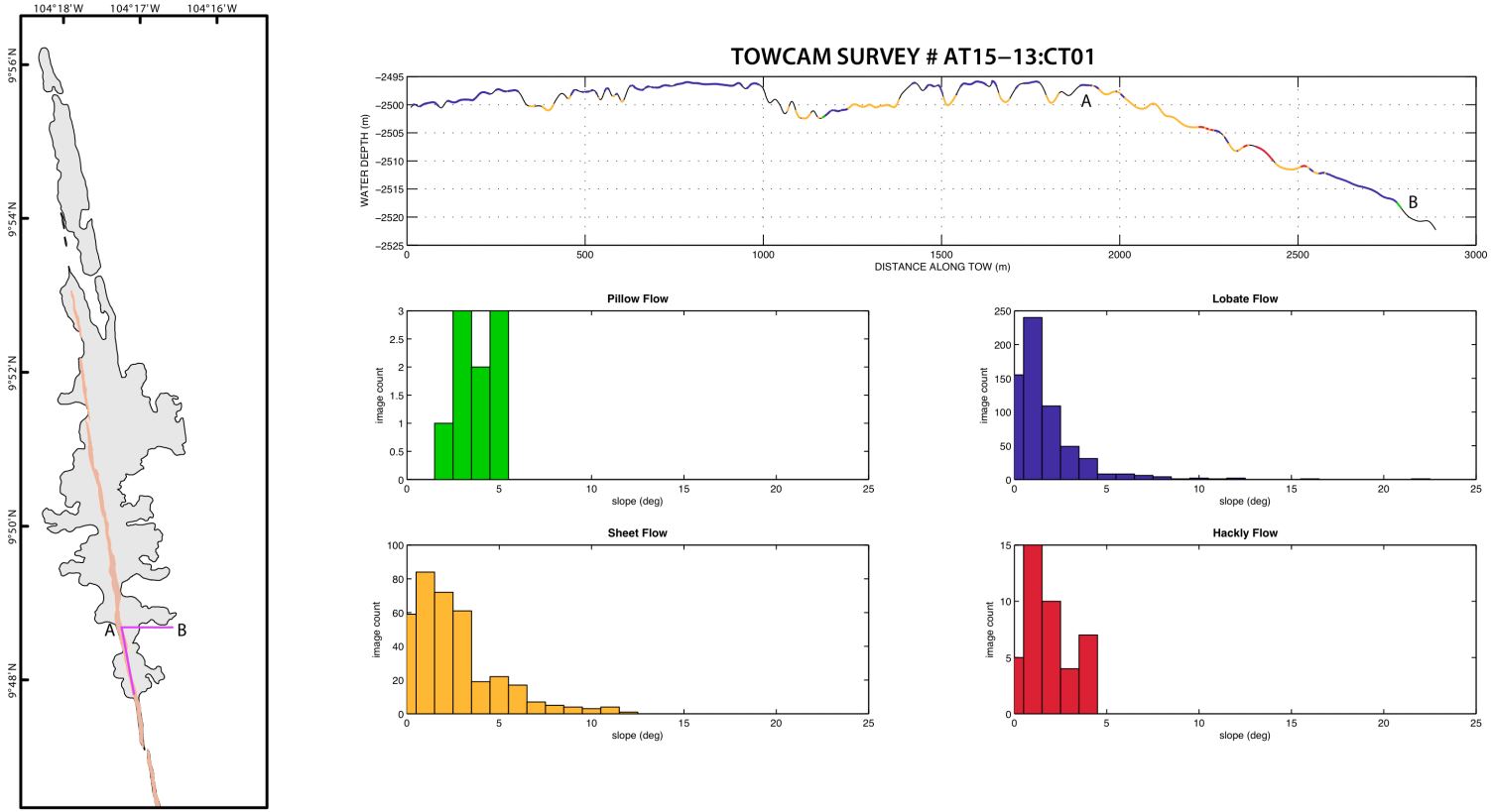

Figure A-4. Inset of map at left showing the position of TowCam survey lines across the 2005–06 EPR eruption. Survey profiles are color coded to flow morphologies: green represents pillow flows, blue represents lobate flows, orange represents sheet flows, and red represents hackly flows. Reference points on the map and profile are marked as A, B and C. The survey profiles show examples of typical across-axis morphological transitions observed in the 2005–06 EPR flows. In this recent eruption, axial erupted lavas formed sheet and lobate flows near the AST and then transitioned into lobate and pillow flows with greater distance from the AST (see text for discussion). Slope calculations are derived from near-bottom TowCam depth profiles. All morphologies occur over the entire range of slopes, indicating that slope created by the 2005–06 EPR eruption did not influence the surface morphology.

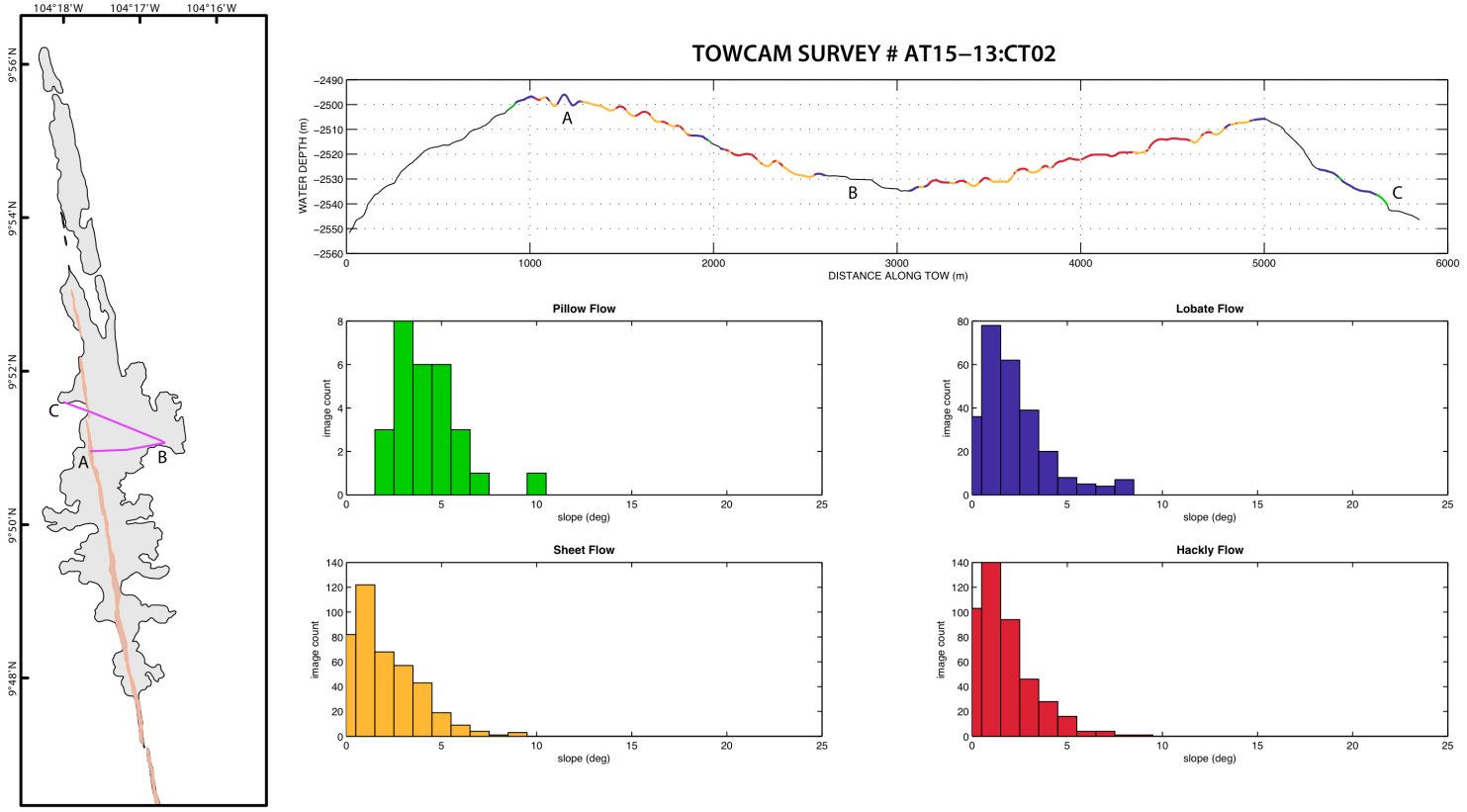

LIST OF REFERENCES

Ballard, R. D., R. T. Holcomb, and T. H. van Andel (1979), The Galapagos Rift at 86˚W: sheet flows, collapse pits, and lava lakes of the rift valley, *J. Geophys. Res*, *84*(B10), 5407-5422.

Ballard, R. D., and T. H. van Andel (1977), Morphology and tectonics of the inner rift valley at lat 36°50'N on the Mid-Atlantic Ridge, *Geo. Soc. America Bull.*, *88*, 507-530.

Ballard, R. D., T. H. van Andel, and R. T. Holcomb (1982), The Galapagos Rift at 86°W 5. variations in volcanism, sturcture, and hydrothermal activity along a 30-kilometer segment of the rift valley, *J. Geophys. Res.*, *87*, 1149-1161.

Blondell, P., and B. J. Murton (1997), *Handbook of Seafloor Sonar Imagery*, 269 pp., John Wiley & Sons, New York.

Bonatti, E., and C. G. A. Harrison (1988), Eruption styles of basalt in oceanic spreading ridges and seamounts: effect of magma temperature and viscosity, *J. Geophys. Res.*, *93*(B4), 2967-2980.

Carbotte, S., and K. Macdonald (1992), East Pacific Rise 8°-10°30'N: evolution of ridge segments and discontinuities from SeaMARC II and three-dimensional magnetic studies, *J. Geophys. Res.*, *97*, 6959-6982.

Carbotte, S. M., M. R. Perfit, J. B. Gill, D. Kelley, J. Canales, M. Nedimovic, and H. D. Carton (2009), Near-axis melt anomalies and segmentation of axial melt: a common framework for the EPR and Endeavor ISS?, *Eos Trans. AGU, 90(52),* Fall Meet. Suppl., Abtract OS11B-01.

Chadwick, W. W., Jr, R. W. Embley, and C. G. Fox (1991), Evidence for volcanic eruption on the southern Juan de Fuca ridge between 1981 and 1987, *Nature*, *350*(6317), 416-418, doi: 10.1038/350416a0.

Chadwick, W. W., Jr., R. W. Embley, and C. G. Fox (1995), SeaBeam depth changes associated with recent lava flows, coaxial segment, Juan De Fuca Ridge: evidence for multiple eruptions between 1981-1993, *Geophys. Res. Lett.*, *22*, 167-170, doi: 10.1029/94GL01895.

Chadwick, W. W., Jr., T. K. P. Gregg, and R. W. Embley (1999), Submarine lineated sheet flows: a unique lava morphology formed on subsiding lava ponds, *Bull. Volcanol.*, *61*(3), 194-206.

Cowen, J. P., D. J. Fornari, T. M. Shank, B. Love, B. Glazer, A. H. Treusch, R. C. Holmes, S. A. Soule, E. T. Baker, M. Tolstoy, and K. R. Pomraning (2007), Volcanic eruptions at the East Pacific Rise near 9°50'N, *Eos Trans. AGU*, *88*(7*),* 81-83, doi: 10.1029/2007EO070001.

Embley, R. W., W. W. Chadwick, Jr., I. R. Jonasson, D. A. Butterfield, and E. T. Baker (1995), Initial results of the rapid response to the 1993 CoAxial event: relationships between hydrothermal and volcanic processes, *Geophys. Res. Lett.*, *22*(2), 143-146.

Embley, R. W., K. M. Murphy, and C. G. Fox (1990), High resolution studies of the summit of Axial Volcano, *J. Geophys. Res.*, *95*, 12,785-712,812.

Engels, J. L., M. H. Edwards, D. J. Fornari, M. R. Perfit, and J. R. Cann (2003), A new model for submarine collapse formation, *Geochem. Geophys. Geosyst.,4*(9), 1077, doi: 10.1029/2002GC000483.

Escartin, J., S. A. Soule, D. J. Fornari, M. A. Tivey, H. Schouten, and M. R. Perfit (2007), Interplay between faults and lava flows in construction of the upper oceanic crust: The East Pacific Rise crest 9˚25´-58´N, *Geochem. Geophys. Geosyst.*, *8*, Q06005, doi: 10.1029/2006GC001399.

Fink, J. H., and R. W. Griffiths (1992), A laboratory analog study of the morphology of lava flows extruded from point and line sources, *J. Volcanol. Geotherm. Res.*, *54*, 19-32.

Fornari, D. J. (2003), A new deep-sea towed digital camera and multi-rock coring system, *Eos Trans. AGU*, *84* (8), 69-76, doi:10.1029/2003EO080001.

Fornari, D. J., R. M. Haymon, M. R. Perfit, T. K. P. Gregg, and M. H. Edwards (1998), Axial summit trough of the East Pacific Rise 9˚-10˚N: geological characteristics and evolution of the axial zone on fast spreading mid-ocean ridges, *J. Geophys. Res.*, *103*(B5), 9,827-9,855.

Fornari, D. J., M. D. Kurz, D. J. Geist, P. D. Johnson, U. G. Peckman, and D. Scheirer (2001), New perspectives on the structure and morphology of the submarine flanks of Galapagos Volcanoes - Fernandina and Isabela, *Eos Trans. AGU, 82*(47) Fall Meet. Suppl., Abstract T41D-06.

Fornari, D. J., M. A. Tivey, H. Schouten, M. Perfit, D. Yoerger, A. Bradley, M. Edwards, R. Haymon, D. Scheirer, K. Von Damm, T. Shank, and A. Soule (2004), Submarine lava flow emplacement at the East Pacific Rise 9 50'N: Implications from uppermost ocean crust stratigraphy and hydrothermal fluid circulation, in *Mid-ocean ridges: Hydrothermal interactions between the lithosphere and oceans*, *Geophys. Monogr. Ser.*, vol. 148, edited by C. R. German, J. Lin, and L. M. Parson, pp.187-218, AGU, Washington, D. C.

Goss, A. R., M. R. Perfit, W. I. Ridley, K. H. Rubin, G. D. Kamenov, S. A. Soule, A. T. Fundis, and D. J. Fornari (in review), Geochemisty of lavas from the 2005–06 eruption at the East Pacific Rise (9°46-56’ N): Implications for decadal changes in magma chamber and mantle compositions, *Geochem. Geophys. Geosyst.*

Gregg, T. K. P., and J. H. Fink (1995), Quantification of submarine lava-flow morphology through analog experiments, *Geology*, *23*, 73-76.

Gregg, T. K. P., and J. H. Fink (2000), A laboratory investigation into the effects of slope on lava flow morphology, *J. Volcanol. Geotherm. Res.*, *96*, 145-159.

Gregg, T. K. P., J. H. Fink, and R. W. Griffiths (1998), Formation of multiple fold generations on lava flow surfaces: Influence of strain rate, cooling rate, and lava composition, *J. Volcanol. Geotherm. Res*, *80*, 281-292.

Gregg, T. K. P., D. J. Fornari, M. R. Perfit, R. M. Haymon, and J. H. Fink (1996), Rapid emplacement of a mid-ocean ridge lava flow on the East Pacific Rise at 9˚46'-51'N, *Earth Planet. Sci. Lett.*, *144*, E1-E7.

Griffiths, R. W., and J. H. Fink (1992), The morphology of lava flows in planetary environments: predictions from analog experiments, *J. Geophys. Res.*, *97*(B13), 19,739-19,748.

Haymon, R. M., D. J. Fornari, M. H. Edwards, S. Carbotte, D. Wright, and K. C. Macdonald (1991), Hydrothermal vent distribution along the East Pacific Rise crest (9˚09'-54'N) and its relationship to magmatic and tectonic processes on fast-spreading mid-ocean ridges, *Earth Planet. Sci. Lett.*, *104*, 513-534.

Haymon, R. M., D. J. Fornari, K. L. Von Damm, M. D. Lilley, M. R. Perfit, J. M. Edmond, W. C. Shanks Iii, R. A. Lutz, J. M. Grebmeier, S. Carbotte, D. Wright, E. McLaughlin, M. Smith, N. Beedle, and E. Olson (1993), Volcanic eruption of the mid-ocean ridge along the East Pacific Rise crest at 9˚45-52'N: direct submersible observations of seafloor phenomena associated with an eruption event in April, 1991, *Earth Planet. Sci. Lett.*, *119*, 85-101.

Hunt, M. M., W. M. Marquet, D. A. Moller, K. R. Peal, W. K. Smith, and R. C. Spindell (1974), An acoustic navigation system, *WHOI Tech. Rep. WHOI-74-6, Woods Hole Oceanogr. Inst.,* Woods Hole, Mass.

Kurras, G. J., D. J. Fornari, M. H. Edwards, M. R. Perfit, and M. C. Smith (2000), Volcanic morphology of the East Pacific Rise crest 9°49′–52′: implications for volcanic emplacement processes at fast-spreading mid-ocean ridges, *Mar. Geophys. Res.*, *21*, 23-41.

Langmuir, C. H., J. F. Bender, and R. Batiza (1986), Petrological and tectonic segmentation of the East Pacific Rise, 5°30'-14°30'N, *Nature*, *322*, 422-429.

Lonsdale, P. (1977), Abyssal pahoehoe with lava coils at the Galapagos rift, *Geology*, *5*, 147-152.

Macdonald, K., J.C. Sempere, and P. J. Fox (1984), East Pacific Rise from Siqueiros to Orozco fracture zones: along-strike continuity of axial neovolcanic zone and stucture and evolution of overlapping spreading centers, *J. Geophys. Res.*, *89*(B7), 6049-6069.

Macdonald, K. C., P. J. Fox, S. Miller, S. Carbotte, M. H. Edwards, M. Eisen, D. J. Fornari, L. Perram, R. Pockalny, D. Scheirer, S. Tighe, C. Weiland, and D. Wilson (1992), The East Pacific Rise and its flanks 8–18° N: history of segmentation, propagation and spreading direction based on SeaMARC II and Sea Beam studies, *Mar. Geophys. Res.*, *14*, 299-344.

Meyer, J., and S. White (2007), Lava morphology mapping by expert system classification of high-resolution side-scan sonar imagery from the East Pacific Rise, 9°–10°N, *Mar. Geophys. Res*, *28*, 81-93.

Milne, P. H. (1983), *Underwater Acoustic Positioning Systems*, *Gulf Publ., Houston, Tex.*
Perfit, M. R., J. R. Cann, D. J. Fornari, J. Engels, D. K. Smith, W. Ian Ridley, and M. H. Edwards (2003), Interaction of sea water and lava during submarine eruptions at mid-ocean ridges, *Nature*, *426*, 62-65.

Perfit, M. R., and W. W. Chadwick (1998), Magmatism at mid-ocean ridges: constraints from volcanological and geochemical investigations, in *Faulting and magmatism at mid-ocean ridges, Geophys. Monogr. Ser.,* vol. 106, edited by W. R. Buck et al., pp. 59-116, AGU, Washington, D. C.

Perfit, M. R., D. J. Fornari, M. C. Smith, J. F. Bender, C. H. Langmuir, and R. M. Haymon (1994), Small-scale spatial and temporal variations in mid-ocean ridge crest magmatic processes, *Geology*, *22*, 375-379.

Rowland, S. K., and G. P. L. Walker (1990), Pahoehoe and aa in Hawaii: volumetric flow rate controls the lava structure, *Bull. Volcanol.*, *52*(8), 615-628.

Rubin, K. H., J. D. Macdougall, and M. R. Perfit (1994), ^{210}Po-^{210}Pb dating of recent volcanic eruptions on the sea floor, *Nature*, *368*, 841-844, doi: 10.1038/368841a0.

Rubin, K. H., M. R. Perfit, D. J. Fornari, S. A. Soule, M. Tolstoy, and F. Wauldhauser (2006), Geochronology and composition of the 2006-06 volcanic eruptions of the East Pacific Rise, 9°46'-56'N, *Eos Trans. AGU, 87,* Fall Meet. Suppl., Abstract V23B-0602.

Rubin, K. H., S. A. Soule, M. R. Perfit, D. J. Fornari, and M. Tolstoy (in prep), Integrating radiometric, geophysical and thermal signals of volcanic unrest and eruption in 2005–06 at 9°50'N EPR, *Geochem. Geophys. Geosyst.*

Rubin, K. H., M. Tolstoy, D. Fornari, R. P. Dziak, S. A. Soule, F. Waldhauser, and K. Von Damm (2008), Integrating radiometric, geophysical and thermal signals of volcanic unrest and eruption in 2005–06 at 9°50'N EPR, *Eos Trans. AGU, 89* Fall Meet. Suppl., Abstract B23F-07.

Sakimoto, S. E. H., and T. K. P. Gregg (2001), Channeled flow: analytic solutions, laboratory experiments, and applications to lava flows, *J. Geophys. Res.*, *106*, 8629-8644.

Scheirer, D. S., D. J. Fornari, S. E. Humphris, and S. Lerner (2000), High-resolution seafloor mapping using the DSL-120 sonar system: quantitative assessment of sidescan and phase-bathymetry data from the Lucky Strike segment of the Mid-Atlantic Ridge, *Mar. Geophys. Res.*, *21*, 121-142.

Schouten, H., M. Tivey, D. Fornari, D. Yoerger, A. Bradley, P. Johnson, M. Edwards, and T. Kurokawa (2002), Lava transport and accumulation processes on EPR 9˚27'N to 10˚N: Interpretations based on recent near-bottom sonar imaging and seafloor observations using ABE, Alvin and a new digital deep sea camera, *Eos Trans. AGU, 83*(47), Fall Meet. Suppl., Abtract T11C-1262.

Shank, T. M., D. J. Fornari, K. L. Von Damm, M. D. Lilley, R. M. Haymon, and R. A. Lutz (1998), Temporal and spatial patterns of biological community development at nascent deep-sea hydrothermal vents (9˚50'N, East Pacific Rise), *Deep Sea Res., Part II, 45*, 465-515.

Sinton, J., E. Bergmanis, K. H. Rubin, R. Batiza, T. K. P. Gregg, K. Gronvold, K. C. Macdonald, and S. M. White (2002), Volcanic eruptions on mid-ocean ridges: new evidence from the superfast spreading East Pacific Rise, 17°-19°S, *J. Geophys. Res.*, *107*(B6), 2115, doi: 10.1029/2000JB000090.

Soule, S. A., K. V. Cashman, and J. P. Kauahikaua (2004), Examining flow emplacement through the surface morphology of three rapidly emplaced, solidified lava flows, Kilauea Volcano, Hawai'i, *Bull. Volcanol.*, *66*, 1-14.

Soule, S. A., D. J. Fornari, M. R. Perfit, W. I. Ridley, M. H. Reed, and J. R. Cann (2006), Incorporation of seawater into mid-ocean ridge lava flows during emplacement, *Earth Planet. Sci. Lett.*, *252*, 289-307.

Soule, S. A., D. J. Fornari, M. R. Perfit, and K. H. Rubin (2007a), New insights into mid-ocean ridge volcanic processes from the 2005-2006 eruption of the East Pacific Rise, 9˚46'N-9˚56'N, *Geology*, *35*, 1079-1082.

Soule, S. A., D. J. Fornari, M. R. Perfit, M. A. Tivey, W. I. Ridley, and H. Schouten (2005), Channelized lava flows at the East Pacific Rise crest 9˚-10˚N: the importance of off-axis lava transport in developing the architecture of young oceanic crust, *Geochem. Geophys. Geosyst.*, *6*, Q08005, doi: 10.1029/ 2005GC000912.

Soule, S. A., S. M. White, D. J. Fornari, V. L. Ferrini, and M. A. Tivey (2007b), Comparison of pre- and post- eruption surveys of the 2005-2006 East Pacific Rise volcanic event: implications for fast-spreading mid-ocean ridge eruption processes, *Eos Trans. AGU, 88(52),* Fall Meet. Suppl., Abstract V21A-0383.

Tolstoy, M., J. P. Cowen, E. T. Baker, D. J. Fornari, K. H. Rubin, T. M. Shank, F. Waldhauser, D. R. Bohnenstiehl, D. W. Forsyth, R. C. Holmes, B. Love, M. R. Perfit, R. T. Weekly, S. A. Soule, and B. glazer (2006), A sea-floor spreading event captured by seismometers, *Science*, *314*, 1920-1922, doi: 10.1126/ science.1133950

Von Damm, K., F. Meana-Prado, J. McDermott, J. Bryce, T. Shank, M. D. Lilley, and D. Fornari (in prep), Seafloor volcanic processes recorded in hydrothermal vent temperature time-series: M vent East Pacific Rise.

Von Damm, K. L., S. E. Oosting, R. Kozlowski, L. G. Buttermore, D. C. Colodner, H. N. Edmonds, and J. M. Edmond (1995), Evolution of East Pacific Rise hydrothermal vent fluids following a volcanic eruption, *Nature*, *375*, 47-50.

White, S. M., R. M. Haymon, and S. Carbotte (2006), A new view of ridge segmentation and near-axis volcanism at the East Pacific Rise, 8°-12°N, from EM300 multibeam bathymetry, *Geochem. Geophys. Geosyst.*, *7*, Q12O05, doi: 10.1029/ 2006GC001407.

White, S. M., R. M. Haymon, D. J. Fornari, M. R. Perfit, and M. Ken C (2002), Correlation between volcanic and tectonic segmentation of fast-spreading ridges: evidence from volcanic structures and lava flow morphology on the East Pacific Rise at 9˚-10˚N, *J. Geophys. Res.*, *107*(B8), 2173, doi: 10.1029/2001JB000571.

BIOGRAPHICAL SKETCH

Allison Tremblay Fundis was born in 1981 in Nashville, TN. She grew up in Nashville and graduated from University School of Nashville in 1999. She earned her B.A. in human ecology with a focus in tropical marine ecology from College of the Atlantic in Bar Harbor, Maine. Upon graduating college, Allison taught high school chemistry and biology at her alma mater, the University School of Nashville. After two years of teaching, she moved with her then boyfriend, now husband, to Gainesville, FL, where he was beginning his PhD at the University of Florida. Allison took a job as a technician working on oceanographic research cruises and instantly fell in love with the sea-going life and marine geology. After discovering she had a newfound interest in geology, she became a laboratory technician for Michael Perfit at UF, aiding him in his geochemical analyses of mid-ocean ridge basalts. This position helped Allison see that she had found a discipline that she was truly excited and passionate about, and so shortly after beginning the position, she enrolled in the graduate program in UF's Department of Geological Sciences. She received her Master of Science degree from UF in the spring of 2010.